IEEE Photonics Journal
An IEEE Photonics Society Publication

Invited Paper

Ultrafast Analog All-Optical Signal Processors Based on Fiber-Grating Devices

Volume 2, Number 3, June 2010

José Azaña

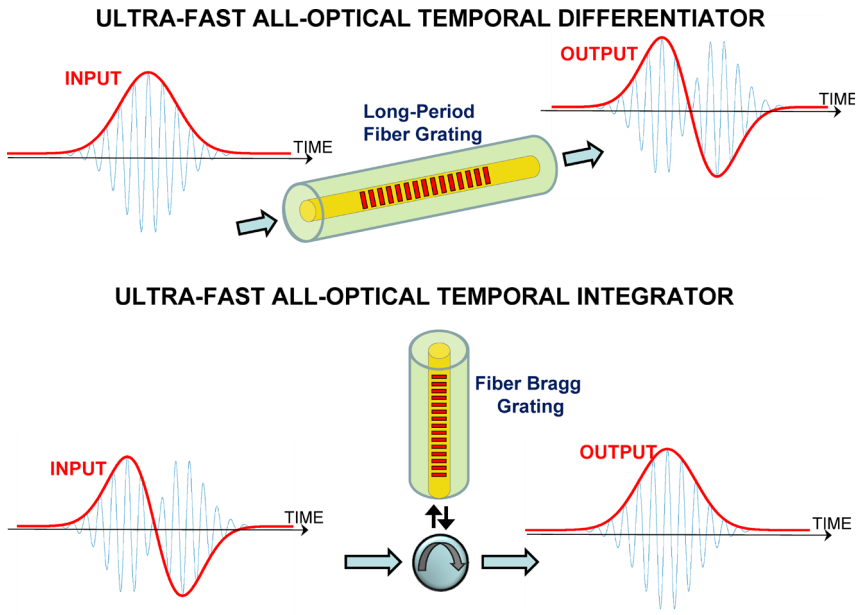

DOI: 10.1109/JPHOT.2010.2047941
1943-0655/$26.00 ©2010 IEEE

Ultrafast Analog All-Optical Signal Processors Based on Fiber-Grating Devices

José Azaña

(Invited Paper)

Institut National de la Recherche Scientifique (INRS), Montreal, QC H5A 1K6, Canada

DOI: 10.1109/JPHOT.2010.2047941

Manuscript received March 4, 2010; revised March 30, 2010. First published Online April 9, 2010. Current version published May 28, 2010. Corresponding author: J. Azaña (e-mail: azana@emt.inrs.ca).

Abstract: This paper reviews recent work on the design, experimental implementation, and application of two fundamental all-optical analog signal processing functionalities, namely, photonic temporal differentiation and photonic temporal integration, using customized grating devices directly written in optical fibers.

Index Terms: Ultrafast devices, fiber gratings, technologies for computing, photonics signal processing, pulse shaping.

1. Introduction

The implementation of all-optical circuits for computing, information processing, and networking could overcome the severe speed limitations currently imposed by electronic-based systems [1]–[3]. A promising approach toward the implementation of ultrafast all-optical circuits is to emulate the developments in the electronic domain, i.e., to follow similar component and design strategies, using photonic technologies. For this purpose, the photonics counterparts of the fundamental devices that form "basic building blocks" in electronic circuits [4]–[6] need to be designed and realized. In electronics, most of basic functionalities like logic operations, differentiation, and integration can be realized using a combination of operational amplifiers, resistors, and capacitors; however, there are still no photonic equivalents to these electronic components. Hence, the design and implementation of these photonic building blocks is a primary step toward the practical realization of all-optical information processing and computing circuits. Two very relevant examples of these fundamental devices are a photonic temporal differentiator [7]–[28] and a photonic temporal integrator [29]–[43].

An Nth-order $(N = 1, 2, 3, \ldots)$ photonic temporal differentiator is a device that provides, at its output, the Nth time derivative of the complex envelope of an input arbitrary optical waveform [7]. The complementary operation is provided by an Nth-order photonic temporal integrator [37], which "calculates" the Nth time cumulative integral of the input temporal complex envelope. It is important to mention that this paper focuses on so-called coherent optical signal processors [7]–[43], in which the relevant processing task is implemented on the complex temporal envelope of the incoming optical signal, including amplitude and phase information. Temporal differentiators [44]–[51] and integrators [52], [53] of time-intensity waveforms (e.g., microwave waveforms transferred into the optical domain) have been also investigated using incoherent photonic signal processing schemes. These have proved particularly useful for the generation and processing of ultrawideband (UWB)

microwave temporal impulse waveforms. Incoherent temporal differentiators and integrators [44]–[53] are, however, outside the scope of the present paper.

Photonic time differentiators were first proposed and theoretically investigated by Ngo *et al.* [7]. They designed arbitrary-order photonic differentiators using integrated-optic transversal filter topologies. To be more concrete, the designs first reported in [7] were based upon finite-impulse-response (FIR) optical digital filters [54]. For instance, it was shown that a first-order photonic differentiator could be implemented using an asymmetric two-arm interferometer (two-tap FIR filter); this device provides the spectral response that is required for optical differentiation over a limited bandwidth centered at any of the destructive resonance frequencies of the interferometer and extending over a fraction of the device free spectral range (FSR) (inversely proportional to the relative delay between the interferometer arms). As an extension of this basic idea, higher order differentiators can be implemented by simply concatenating in series the corresponding number of identical two-arm interferometers. A large number of subsequently developed photonic differentiators both for complex-field optical waveforms [11], [13], [24] and for intensity signals [44]–[51] are based on this general concept.

Following this pioneer work, Kulishov and Azaña [8] found out that first-order time differentiation could be inherently provided by a simple *uniform* long-period fiber grating (LPG) operating in full-coupling condition. By "uniform" we refer to the simplest possible grating profile, having an amplitude and period that are both constant along the whole grating length. An LPG [55] allows light coupling between the guided mode and cladding modes in a single-mode fiber, thus resulting in a series of spectrally broad attenuation (resonance) bands centered at discrete wavelengths (frequencies) in the fiber transmission spectrum. The term "long" refers to its period, which typically varies from tens to hundreds of micrometers, as opposed to short-period fiber gratings (fiber Bragg gratings (FBGs) [56]), where the light is backscattered, resulting in coupling between modes traveling in opposite directions (in a Bragg geometry, the corrugation period is approximately half the optical wavelength, in micrometers or less).

The original proposal of a simple uniform LPG for optical differentiation [8] has inspired a significant amount of subsequent work on the design and realization of ultrafast photonic temporal differentiators and integrators based on fiber-grating devices (both LPGs and FBGs). The advantages of fiber gratings are intrinsic to their all-fiber geometry, namely simplicity, relatively low cost, low losses, and full compatibility with fiber optic devices and systems. Additionally, fiber-grating concepts could be transferred to integrated-optic platforms [57], as desired for the future development of monolithic ultrafast all-optical processing circuits. Moreover, LPG and FBG technologies have attracted considerable interest over the last years due to their very wide range of applications in fiber-optic telecommunication systems, ultrafast optical pulse processing and shaping, and optical sensing [56]; as a result, fiber-grating technologies have reached a high level of maturity, and efficient and advanced design and fabrication methods are now readily available. It should be mentioned that volume Bragg gratings have also been recently explored for optical differentiation as an interesting alternative to all-fiber gratings for high-power applications [28].

Besides its simplicity, a very attractive feature of an LPG-based differentiator is the large processing bandwidth practically attainable with this solution, namely, in the terahertz range [8], [17]. LPG differentiators can thus easily process optical signal with time features down to the sub-picosecond range. The first experimental demonstration of an ultrafast all-optical differentiator was based on this solution [9], which is reviewed in Section 2.1 below. Reflection FBGs, e.g., phase-shifted FBGs [12], [14], sampled FBGs designed according to a reconstruction-equivalent-chirp method [19], and apodized FBGs [26] designed by general layer-peeling synthesis algorithms [58], can be tailored to achieve the spectral responses that are necessary for first-order and higher order optical differentiators; however, besides requiring the use of nonuniform grating profiles, the resulting FBG designs are practically limited to processing bandwidths that are typically < 50 GHz. Solutions based on especially apodized linearly chirped FBGs (LC-FBGs) have been explored to overcome the severe bandwidth limitations of conventional FBG designs [16], [18]. A particularly interesting approach is based on especially apodized LC-FBGs operated in transmission [16]; this approach, which is reviewed in Section 2.2, has been experimentally demonstrated to constitute a

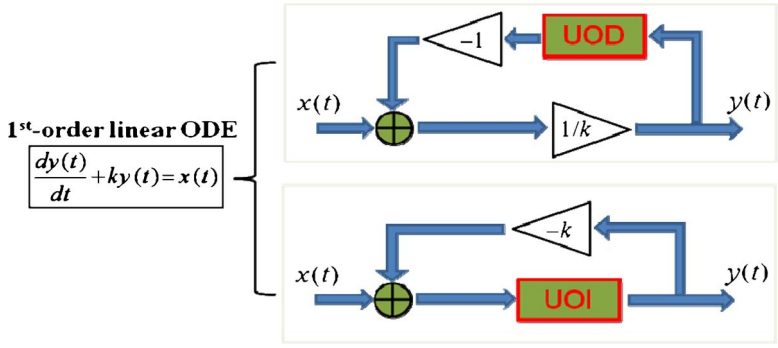

Fig. 1. Analog all-optical computing schemes for real-time solving of a first-order linear ODE using an ultrafast optical differentiator or an ultrafast optical integrator.

practical and efficient solution for implementing all-fiber high-order temporal differentiators with operational bandwidths approaching the terahertz regime [25].

Concerning photonic temporal integrators, solutions have been proposed using active or passive resonant cavities [29]–[35], i.e., feedback-based optical filters, including designs based on passive phase-shifted FBGs operated in transmission [32], [33] and an active resonant cavity based on superimposed LC-FBGs photo-inscribed in an Er-Yb-codoped optical fiber [34]. This latter design has been experimentally demonstrated. Resonant-cavity-based photonic integrators can be designed using a general infinite-impulse-response (IIR) (for active devices) or FIR (for passive devices) optical digital filter approach [54]. The main drawback of resonant-cavity-based photonic integrators [29]–[35] is that they exhibit a fundamental limitation on the operation frequency bandwidth, which is inherently limited by the characteristic FSR of the used cavity (typically smaller than a few tens of gigahertz). Single passive-reflection FBG filters have been designed to implement first- and high-order photonic temporal integrators capable of providing processing bandwidths up to the terahertz range [36]–[40]. The main drawback of any passive temporal integrator is that it necessarily operates over a limited time window. A particularly simple and efficient time-limited integrator design is based on the use of a reflection FBG emulating the time impulse response of an ideal integrator over a finite time window (operational time window of the device) [36], [37]. Based on this approach, a first-order temporal integrator can be implemented using the simplest possible FBG, i.e., a weak-coupling uniform FBG [36]. This solution is discussed in detail in Section 3.1. As a generalization of this basic idea, first- and high-order integrators with optimized energetic efficiencies and offering operational time windows in the nanosecond range can be implemented using uniform-period FBGs with properly tailored grating apodization profiles [40]. This generalized solution for arbitrary-order temporal integration is discussed in Section 3.2.

In analogy with their electronic counterparts, photonic temporal differentiators and integrators are key elements to create a large variety of information processing and computing platforms [4]–[6]. A very relevant example of application of these fundamental devices is that of analog computing systems devoted to solving ordinary differential equations (ODEs) [4]. These equations play a central role in virtually any field of science or engineering [59], e.g., physics, chemistry, biology, economics, medical sciences, and the different branches of engineering. It is well known that linear ODEs can be solved in real time using a suitable combination of temporal differentiators and/or temporal integrators, adders, and multipliers (amplifiers/attenuators) [4]. The possibility of realizing these computations all-optically translates into potential processing speeds well beyond the reach of present electronic digital or analog computers. Fig. 1 illustrates an example of all-optical computation of a constant-coefficient linear first-order ODE using either a first-order ultrafast optical differentiator (UOD in the figure) or a first-order ultrafast optical integrator (UOI in the figure). Notice that this simple differential equation actually models a number of important engineering systems and physical phenomena [59], including problems of motion subject to acceleration inputs and

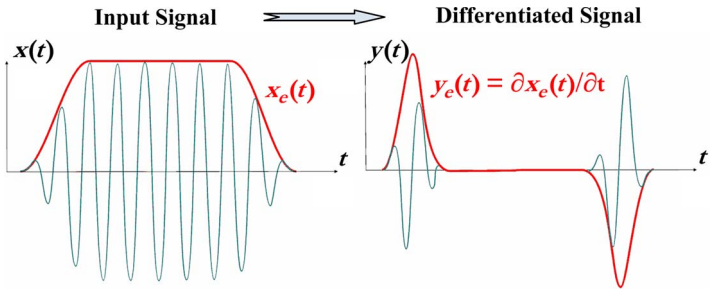

Fig. 2. Operation of an ideal photonic differentiator on an input arbitrary optical signal.

frictional forces, temperature diffusion processes, response of different RC circuits, population dynamics in biology and economy, etc.

Beyond their intrinsic importance for general optical computing and information processing tasks, photonic differentiators and integrators implement fundamental mathematical operations on ultrafast optical temporal waveforms, thus being of interest for a wide range of applications, including optical/microwave pulse shaping [7], [9], [10], [39], [60]–[62], ultrafast optical control and sensing [7], ultrahigh-speed photonic coding and decoding [13], [39], ultrafast optical signal measurements [63], [64], photonic device characterization [65], implementation of optical memory units [35], [45], [66], etc. Some of these applications are briefly discussed in Sections 2.3 and 3.3.

2. Ultrafast Photonic Temporal Differentiators

2.1. First-Order Photonic Differentiators Based on LPGs

2.1.1. Operation principle

A first-order photonic temporal differentiator is a device that "calculates" the first time derivative of the complex envelope of an incoming arbitrary optical waveform; see Fig. 2.

Let us assume an arbitrary optical signal spectrally centered at the optical frequency ω_0 (carrier frequency). The signal's time-domain representation can be mathematically described as follows: $x(t) = \mathrm{Re}\{\hat{x}(t)\} = \mathrm{Re}\{x_e(t)e^{j\omega_0 t}\}$, where $\hat{x}(t)$ is the analytic representation, and $x_e(t)$ is the complex temporal envelope of the optical signal. Notice that it is assumed that the slow-varying envelope approximation always holds for the involved optical signals (i.e., the spectral bandwidth of the signal under analysis is much smaller than the carrier frequency). The output from an ideal photonic differentiator when $x(t)$ is launched at its input should be an optical signal $y(t)$ spectrally centered at the same carrier frequency ω_0 and with a complex temporal envelope proportional to the first-time derivative of the input complex envelope, i.e., $y(t) = \mathrm{Re}\{\hat{y}(t)\} = \mathrm{Re}\{y_e(t)e^{j\omega_0 t}\}$, where $y_e(t) \propto \partial x_e(t)/\partial t$ (the symbol $\propto$ holds for proportionality).

The above relationship between the input and output temporal envelopes can be expressed in the frequency domain using the well-known Fourier transform of the derivative operator [4], $Y_e(\omega) \propto j\omega X_e(\omega)$, where $X_e(\omega)$ and $Y_e(\omega)$ are the Fourier transforms (complex spectra) of the input and output temporal envelopes, $x_e(t)$ and $y_e(t)$, respectively. In this notation, $\omega = \omega_{opt} - \omega_0$ is the baseband angular frequency variable, with ω_{opt} being the optical angular frequency variable. Thus, in terms of the signals' analytic representations, $\hat{Y}(\omega_{opt}) \propto j(\omega_{opt} - \omega_0)\hat{X}(\omega_{opt})$. The latter relationship indicates that the ratio $\hat{Y}(\omega_{opt})/\hat{X}(\omega_{opt}) \propto j(\omega_{opt} - \omega_0)$ is independent on the input optical signal (i.e., it is fixed for any given arbitrary input optical waveform). This in turn implies that the desired differentiation operation can be practically implemented using a linear optical filter providing a spectral transfer function $\hat{H}_1(\omega_{opt}) \propto j(\omega_{opt} - \omega_0)$. In practice, this transfer function will extend over a limited spectral bandwidth (centered at ω_0), which ultimately determines the processing speed of the photonic differentiator. The two key features of the required filter's transfer function are that i) it depends linearly on the baseband frequency and that ii) it is zero at the signal

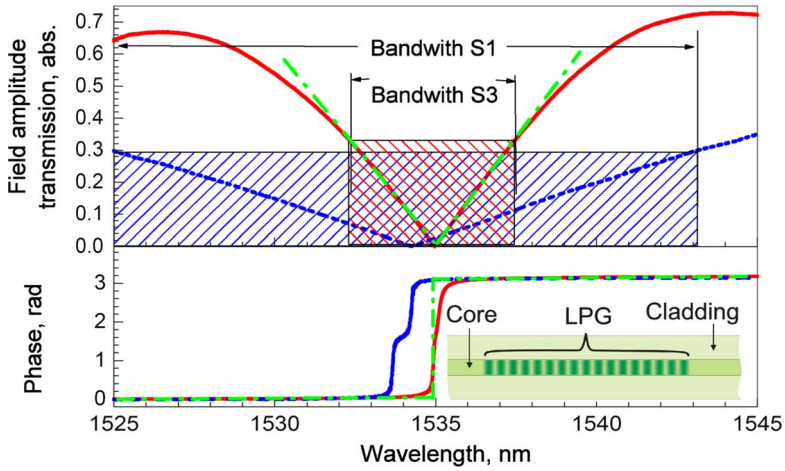

Fig. 3. Amplitude and phase characteristics of the fiber LPG filters. Measured field amplitude and phase characteristics of the realized long S3 (red) and short S1 (blue) LPGs, together with the theoretical characteristics of an ideal differentiator similar to S3 (green, dash-dotted lines). The S3 and S1 LPG operational bandwidths (highlighted in the figure) are 5.5 nm and 19 nm, respectively. The inset shows a fiber uniform LPG, where the level of green corresponds to the refractive index (from [9]).

central frequency ω_0. It is worth noting that these two key features imply an exact π phase shift across the central frequency ω_0. The ideal complex transfer function of an optical differentiator is shown in Fig. 3 (dash-dotted green line).

An ideal photonic differentiator requires complete energy depletion at the signal central frequency. This can be produced by a resonance-induced full energy transfer elsewhere. Specifically, in waveguide optics, this can be achieved by resonant transfer of light between two spatially close waveguides, or between two modes of the same waveguide (e.g., cladding and core modes or counter-propagating core modes of an optical fiber). Resonant light coupling is induced when the light propagates through both waveguides (modes) with identical speeds, which is practically attainable e.g., by an increase or decrease of the light speed in one of the waveguides (modes) using a suitable diffraction grating [55], [56]. In particular, we anticipated that the desired spectral characteristics for temporal differentiation are provided "inherently" by the core's transfer function of a single uniform LPG (around its resonance frequency, ω_R) when the grating is designed to operate at full-coupling conditions [8].

An LPG, which is practically realized as a periodic change of the refractive index along the direction of light propagation within an optical fiber, induces gradual resonant coupling at a rate of κ per unit length between the core guided mode and cladding mode(s) [55]. To obtain efficient coupling between these modes, the period of the LPG must be properly adjusted to cause light diffraction from the core mode into the chosen cladding mode. In particular, resonant coupling occurs when the following condition is satisfied: $\sigma(\omega_{opt}) = [\beta_{co}(\omega_{opt}) - \beta_{cl}(\omega_{opt})]/2 - (\pi/\Lambda) = 0$, where $\sigma(\omega_{opt})$ is referred to as the detuning factor, $\beta_{co}(\omega_{opt})$ and $\beta_{cl}(\omega_{opt})$ are the propagation constants for the interacting core and cladding modes, respectively, c is the speed of light in a vacuum, and Λ is the physical grating period. Due to the different dispersion slopes of the two interacting modes, the given resonant coupling condition $(\sigma = 0)$ is strictly satisfied at a specific frequency, $\omega_{opt} = \omega_R$, referred to as the LPG resonance frequency. From coupled-mode theory [55], the core spectral transmission response of a uniform LPG (assuming that the input pulse propagates along the fiber core mode) can be expressed as follows:

$$\hat{H}_{co}(\omega_{opt}) = \left[\cos(\gamma L) + j\frac{\sigma}{\gamma}\sin(\gamma L)\right]\exp(j(\beta_{co} - \sigma)L) \quad (1)$$

where $\gamma = \sqrt{\sigma^2 + \kappa^2}$ and L is the total grating length. The transmission function in Eq. (1) can be approximated in the vicinity of the resonance frequency ω_R (where $\sigma \rightarrow 0$) by the two first nonzero terms of the corresponding Taylor series expansion

$$\hat{H}_{co}(\omega_{opt}) \approx \left[\cos(\kappa L) + j\frac{\sigma}{\kappa}\sin(\kappa L)\right]\exp(j\beta_{co,0}L) \tag{2}$$

where $\beta_{co,0} = \beta_{co}(\omega_R)$, and $\sigma(\omega_{opt}) \approx \sigma_1(\omega_{opt} - \omega_R)$, with $\sigma_1 = (1/2)[\partial\beta_{co}(\omega_R)/\partial\omega_{opt} - \partial\beta_{cl}(\omega_R)/\partial\omega_{opt}]$. It is known that if the device is designed to exactly satisfy the so-called full-coupling condition, $\kappa L = m(\pi/2)$, with $m = 1, 3, 5, \ldots$, then the grating induces a total (100%) energy coupling from the input-guided core mode into the cladding mode (at ω_R) [67]. Under this condition, Eq. (2) can be approximated by $\hat{H}_{co}(\omega_{opt}) \propto j\sigma \propto j(\omega_{opt} - \omega_R)$. Thus, as anticipated, an uniform LPG operating in full-coupling condition provides, around its resonance frequency, the spectral transmission linear dependence that is necessary for first-order time differentiation, including the required zero transmission and the associated π phase shift at the resonance frequency ω_R. This device will thus operate as a first-order time differentiator over any arbitrary input optical signal centered at the LPG resonance frequency, i.e., $\omega_0 = \omega_R$, as long as the signal's frequency content extent over a bandwidth narrower than that over which the LPG transmission exhibit a linear response (i.e., spectral bandwidth over which the above Taylor series approximation is valid).

Two important parameters to evaluate the performance of a general optical processor, including photonic differentiators [7], are the processing error, which is defined as the deviation between the actually obtained and the ideal temporal signal profile at the processor output, and the energetic efficiency, which is defined as the ratio between the output signal energy and the input signal energy. For a given LPG differentiator, these two performance parameters strongly depend on the spectral bandwidth of the input signal to be processed [8]. In particular, differentiation of faster temporal features (i.e., signals with larger bandwidths) is usually achieved with a higher energetic efficiency but at the expense of a higher processing error. This is expected considering that the spectral transmission response of the LPG resonance deviates further from the ideal linear-amplitude variation as the frequency relative to the resonance center is increased. In contrast, narrower bandwidth signals are differentiated with a higher accuracy but at the expense of a poorer energetic efficiency. The latter can be attributed to the fact that the spectral components closer to the resonance frequency are more strongly attenuated after propagation through the LPG filter, i.e., a larger portion of the input pulse spectrum will be filtered out when processing a pulse with a narrower frequency bandwidth. Generally speaking, optical differentiators are intrinsically inefficient devices from an energetic viewpoint; this is again associated with the fact that the input signal spectral content is strongly attenuated by the LPG filter particularly around the signal's carrier frequency, where most of the signal energy is typically concentrated for practical optical waveforms (e.g., Gaussian-like optical pulses). The device energetic efficiency can be increased by photo-inscribing the LPGs in active optical fibers [22], e.g., in Er-doped optical fibers, in which simultaneous amplification of the propagating signal can be obtained by pumping the fiber medium with suitable CW light. The advantages of such an implementation over the setup using concatenation of a passive LPFG with an amplifier lies in reducing the unwanted nonlinearities and reducing the amplified spontaneous emission (ASE). Active-fiber-based LPG first-order photonic temporal differentiators with power efficiencies surpassing 100% have been experimentally demonstrated [22].

In Fig. 4, we numerically evaluated the maximum signal spectral bandwidth that can be differentiated using uniform LPGs of different lengths in order to ensure that the relative processing error is kept lower than 1% (see details of this numerical evaluation in [8]). The analysis was made considering feasible grating lengths ranging from 2 cm to 10 cm. As expected, the shorter the LPG, the larger the processing bandwidth it provides. It is important to note that ultrafast signals with temporal features in the subpicosecond regime (corresponding bandwidths $>$ 1 THz) could be processed using uniform LPGs of a few centimeters long.

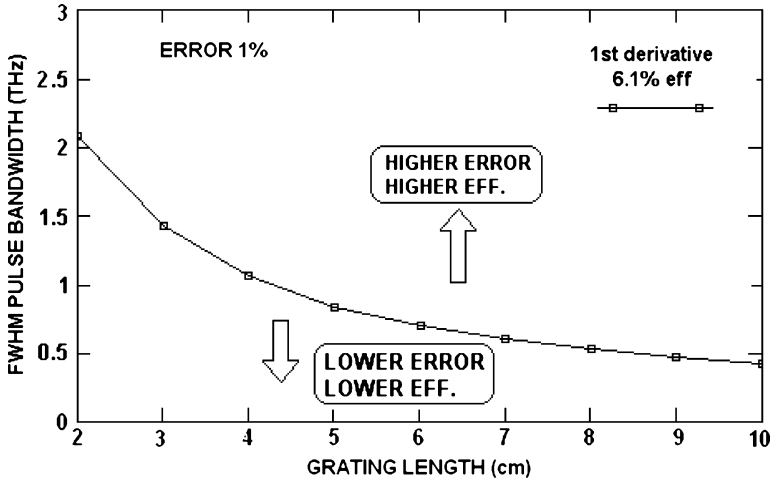

Fig. 4. Maximum signal bandwidth (FWHM bandwidth of input Gaussian pulse) that can be processed with a uniform LPG operated as a first-order differentiator (solid-box curve) to keep the processing error lower than 1%, evaluated for different grating lengths (from [8]).

The fact that a single *uniform* LPG provides just the spectral features required for optical differentiation around its resonance frequency over such large spectral bandwidths (terahertz range) is an extraordinary and fortunate occurrence which cannot be generalized to other types of basic resonant structures. For instance, the spectral shape of the resonance induced in the transmission response of a uniform FBG—induced by energy coupling from the signal-carrying fiber mode into the counter-propagating mode—strongly deviates from the linear-amplitude shape that is required for first-order time differentiation. It has been suggested that a suitable apodization of the grating refractive index profile, resulting in a strongly nonuniform FBG profile, could be introduced to obtain the desired linear-amplitude variation in the grating's spectral transmission response [16], [21]. The use of an additional grating chirp would also help to increase the resonance (i.e., differentiation) bandwidth [16]. Considering that time differentiators are intrinsically minimum phase filters [21], it has been argued that the required π phase shift at the resonance frequency would be inherently obtained in the FBG transmission response for a sufficiently strong resonance dip (i.e., if the filter transmission at the resonance frequency approaches very nearly the required zero value). In particular, it has been estimated that a resonance dip stronger than $\sim$50 dB would be required to achieve a first-order time differentiator with a reasonable performance. This is an immensely challenging practical requirement, resulting in unpractical grating amplitude profiles. The use of a concatenated reflection phase-shifted FBG has been proposed as a potential solution to achieve the required specifications (i.e., π phase shift) at the resonance frequency [16]; however, this solution would drastically limit the operational bandwidth of the differentiator device as practical phase-shifted FBGs are typically limited to full-reflection bandwidths $<$ 100 GHz.

2.1.2. Experimental results

To fabricate an LPG-based optical differentiator, stringent control of the fiber LPG coupling strength (which must be fixed exactly at $\kappa L = \pi/2$) is required. The two LPG samples discussed here [68] were fabricated by Slavík at the *Academy of Sciences of the Czech Republic*. They were made in a standard fiber sample (SMF-28, Corning Inc.), using the established point-by-point technique with a CO_2 laser [69]. These two LPG examples have physical lengths of 2.6 cm (sample S1) and 8.9 cm (sample S3), and a grating period of 415 μm. Based on numerical analysis [55], this grating period corresponds to coupling into the fifth odd cladding mode at a resonance wavelength of 1540 nm. The amplitude and phase characteristics of these fiber LPG filters were measured by an Optical Vector Analyzer (Luna Technologies) and are shown in Fig. 3. The linear and quadratic

terms in the phase curve—caused by the delay and linear chromatic dispersion, respectively—have been subtracted. The LPGs exhibited an extremely deep attenuation, breaking the 60-dB limit, confirming operation at almost exact full-coupling condition, as required by our application. In fact, we measured a nearly exact π phase shift at the filter resonance wavelength. The "operational" bandwidths of the fabricated LPGs were approximately 19 nm (S1) and 5.5 nm (S3). Notice that the "operational" bandwidth is the LPG resonance bandwidth over which the fiber filter provides the desired linear-amplitude filtering function. This corresponds approximately to the bandwidth over which the LPG transmission (in intensity) is lower than 10%. Assuming input Gaussian pulses, these LPG samples could be used to process pulses as short as 700 fs (S3) and 180 fs (S1), where we considered the LPG operational bandwidth matched to the pulse bandwidth given at 10% of its peak power. The attainable processing bandwidth of a LPG-based optical differentiator is ultimately limited by the presence of a slight nonlinear dispersion slope of the core and cladding modes, which starts to deform the resonance linear shape when a large bandwidth is considered—using numerical simulations, we estimated that a differentiator made in a standard telecom fiber could operate up to 10-THz speeds (Gaussian pulses down to 60 fs); the corresponding LPG length is 1 cm. For higher speeds, a special fiber with engineered core/cladding mode dispersion or an apodized LPG would be needed.

The fabricated devices were successfully demonstrated for time differentiation of ultrafast optical signals, particularly subpicosecond optical pulses. Notice that in the demonstrations reported here, we used the optical differentiator based on the long LPG sample S3, because the bandwidth of this LPG was better matched to the bandwidth of the optical pulses generated by the available laser, ensuring a higher energetic efficiency in the differentiation process. For an input pulse source, we used a passively mode-locked wavelength-tunable fiber laser (Pritel Inc., USA), which generated nearly transform-limited Gaussian-like optical pulses with a FWHM time width of $\approx$700 fs at a repetition rate of 20 MHz. The pulses were centered at the LPG resonance wavelength of 1535 nm. Because the LPGs are slightly birefringent, the light from the laser was passed through a fiber polarization controller and then directly launched into LPG for time differentiation. We employed a fiber-based Spectral Interferometry (SI) technique [70] to fully characterize the amplitude and phase of the differentiated optical pulses (i.e., pulse waveforms at the LPG output). The specific details of the used measurement setup can be found in [71]. Briefly, an imbalanced Mach–Zehnder interferometer was formed by two fiber couplers; the fiber differentiator was put into one of its arms together with two polarization controllers for polarization control of the light incident to the component and of the interferometer. The spectral pattern resulting from interference between the input (reference) optical pulse and the waveform at the differentiator output was captured at the interferometer output using an optical spectrum analyzer (OSA); this interference pattern was used for reconstruction of the amplitude and phase time profiles of the waveform generated at the differentiator output. For this purpose, the well-known Fourier Transform SI algorithm was applied [70]. Fig. 5 presents the results of one of these measurements together with the theoretical predictions (numerical derivative of an ideal 700-fs Gaussian pulse, whose temporal intensity profile is shown with a dotted curve). We observe an excellent agreement between the theory and the experiment and in particular, as expected for a Gaussian input pulse, an odd-symmetry Hermite–Gaussian (OS-HG) waveform, consisting of two consecutive pulses in antiphase, was generated at the differentiator output. Each peak (FWHM $\approx$ 500 fs) of the generated temporal waveform was slightly narrower than the original Gaussian (FWHM $\approx$ 700 fs), and our measurements clearly confirmed the predicted presence of an almost exact *discrete* π phase shift between the two temporal lobes of the generated OS-HG waveform. Notice also that the peaks of the two lobes in the generated waveform are temporally separated by $\approx$900 fs and that they have slightly different amplitudes (5% in terms of relative intensities). This difference is caused by a slight deviation of the LPG spectral filtering characteristic from the ideal (linear) distribution.

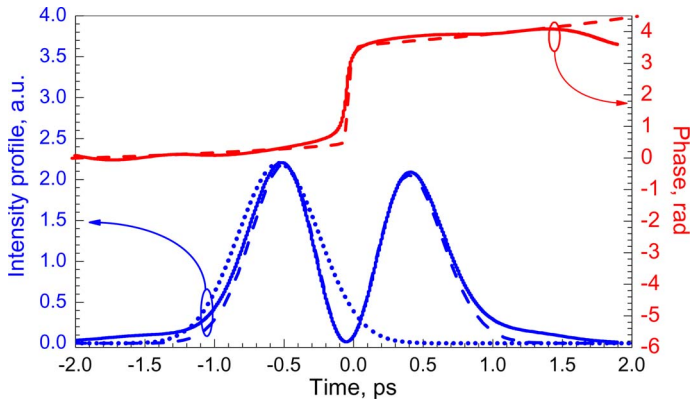

Fig. 5. Results from Spectral Interferometry (SI) measurements. The phase (red) and intensity (blue) temporal profiles of the generated odd-symmetry HG waveform are retrieved from the experimental data obtained using Fourier-Transform SI (solid lines); the theoretical prediction (dashed lines) and considered input pulse waveform (dotted line) are also shown (from [9]).

2.2. High-Order Photonic Differentiators Based on FBGs

An *N*th-order photonic differentiator is a device that provides the *N*th time derivative of the time complex envelope of an input arbitrary optical waveform [7]. Our analysis here is focused on integer-order differentiators, i.e., when $N = 1, 2, 3, \ldots$; notice that fractional-order differentiators, in which *N* is extended to be any real positive number, have been also recently designed using FBGs [23]. Using the same notation as above, the temporal complex envelope, $y_e(t)$, of the optical signal at the output of an ideal *N*th-order differentiator when a signal with a complex envelope $x_e(t)$ is launched at its input is given by $y_e(t) \propto \partial^N x_e(t)/\partial t^N$. Both input and output signals are spectrally centered at the same optical frequency ω_0. Following a similar development to that detailed above for a first-order differentiator, it can be easily proved that an *N*th-order photonic differentiator can be implemented using a linear optical filter providing a spectral transfer function $\hat{H}_N(\omega_{opt}) \propto j(\omega_{opt} - \omega_0)^N$. Thus, considering that optical differentiation is a purely linear, time-invariant process, an *N*th-order optical differentiator could be implemented by connecting in series *N* first-order optical differentiators [7], [13]. This can for instance be achieved by simply concatenating *N* uniform LPGs, each one operating in full-coupling conditions, along the same optical fiber [15]. In practice, some additional technique need to be used in between the gratings in order to remove, or significantly attenuate, the energy coupled into the cladding mode by the LPGs (e.g., by deposition of a high-refractive-index layer).

Obviously, the use of concatenated first-order differentiators translates into several important drawbacks, including an increased implementation complexity and a decrease of the device's energetic efficiency for higher differentiation orders. Several fiber-grating solutions have been investigated to create an ultrafast arbitrary-order differentiator using a minimum number of concatenated devices (even a single all-fiber device, if possible) [16]–[18]. An interesting solution is based on the use of multiple phase-shifted LPGs [17]; in particular, it has been theoretically shown that an LPG consisting of *N* grating segments, each of them formed by a uniform LPG, with π-phase shifts between them, can be designed to perform the *N*th-order differentiation by properly fixing the relative lengths of the different grating sections as well as the LPG coupling strength. As expected for LPG filters, this solution can offer operational bandwidths well in the terahertz range (multiple-phase-shifted FBGs operated in reflection have been also suggested for high-order differentiation [14] but they are severely limited to operation bandwidths that are typically < 20 GHz). The main challenge in applying the phase-shifted method to the LPG-based high-order differentiators is in the extremely high precision with which the LPG inscription has to be controlled to achieve the desired functionality, e.g., to achieve the required resonance attenuation > 50 dB. Second-order differentiators based on this method have been experimentally demonstrated [27], but it has proved challenging to fabricate phase-shifted LPGs for higher order differentiation operations.

2.2.1. Operation principle and FBG design

An alternative approach based on the use of especially apodized LC-FBGs operated in transmission [25], is described here in more detail. Considering the spectral transfer function of an Nth-order photonic differentiator $\hat{H}_N(\omega_{opt}) \propto j(\omega_{opt} - \omega_0)^N$, one can easily infer that for even-order differentiator (i.e., for $N = 2, 4, 6, \ldots$), the filter should modify only the spectral amplitude of the input optical signal, i.e., a customized amplitude-only optical filtering operation, $\hat{H}_N(\omega_{opt}) \propto |\omega_{opt} - \omega_0|^N$, should be implemented. A broadband amplitude-only optical linear filter providing a fully customized amplitude transfer function can be realized using a single especially apodized LC-FBG operated in transmission [72]. In the case of an odd-order differentiator, besides a customized amplitude spectral response, the filter should also introduce an exact π phase shift at the signal's carrier frequency, ω_0. Notice that at this specific frequency, which will referred to as the device's resonance frequency, the filter response should always approach to zero, regardless of the differentiation order. As discussed above for the case of first-order differentiators, the use of a concatenated reflection phase-shifted FBG was first proposed as a potential solution to achieve the required π phase shift at the resonance frequency [16]; however, this solution would limit the operational bandwidth of the differentiator device as practical phase-shifted FBGs are typically limited to full reflection bandwidths that are < 100 GHz. A simpler and more efficient solution for implementing an arbitrary odd-order photonic differentiator (i.e., for $N = 3, 5, \ldots$) is based on the fact that in this case, the required filtering function can be implemented as a concatenation of a first-order differentiator and the immediately lower even-order differentiator, i.e., mathematically $\hat{H}_N(\omega_{opt}) \propto \hat{H}_1(\omega_{opt})\hat{H}_{N-1}(\omega_{opt}) = \hat{H}_1(\omega_{opt})|\omega_{opt} - \omega_0|^{N-1}$. The first-order device can be implemented using a uniform LPG (intrinsic transmission device), whereas the latter can be practically realized using a single especially apodized LC-FBG operated in transmission implementing the amplitude-only spectral transfer function defined by $\hat{H}_{N-1}(\omega_{opt}) \propto |\omega_{opt} - \omega_0|^{N-1}$. This scheme allows one to realize any desired differentiation order using a maximum of two concatenated fiber-grating devices, both operating in transmission.

A broadband optical filter with a tailored amplitude spectral response can be realized using an especially apodized LC-FBG operated in transmission [72]. The design relationships in such an optical filter are illustrated in Fig. 6. Consider and apodized LC-FBG with a constant effective refractive index, n_{av}, a normalized grating apodization profile $A(z)$ (variation of the refractive-index modulation as a function of the distance along the fiber axis z), a grating period chirp $C_K = \Delta K/\Delta z$, where ΔK is the angular spatial frequency variation over a fiber distance Δz, and a total fiber-grating length L. The linear spatial-frequency variation of the grating along the fiber length induces a linear group delay in the FBG's reflection spectral response. If the grating-induced dispersion (slope of the reflection group delay) is sufficiently large, then it is fair to assume that a single frequency is reflected at each single location along the grating length, as determined by the corresponding Bragg condition; under this assumption, the amplitude of the spectral response at each frequency within the FBG reflection bandwidth depends only on the grating coupling strength at the corresponding location, as determined by the apodization profile $A(z)$. As a result, the magnitude of the FBG transmission spectral response, $\hat{H}_{tx}(\omega_{opt})$, is tailored following the grating apodization profile according to the following equation [72]:

$$\left|\hat{H}_{tx}(\omega_{opt})\right| \propto \sqrt{1 - \tanh^2\left[mA\left(z = \frac{2n_{av}}{cC_K}(\omega_{opt} - \omega_0)\right)\right]}, -L/2 \leq z \leq L/2 \tag{3}$$

where m is an arbitrary constant, and $\omega_0 = \pi c/(n_{av}\Lambda_0)$ is the Bragg frequency at $z = 0$, which is fixed by the central grating period $\Lambda_0 = \Lambda(z = 0)$. In our designs of optical differentiators, the LC-FBG needs to be properly apodized so that to obtain the amplitude filtering function corresponding to the desired differentiation order, i.e., $|\hat{H}_{tx}(\omega_{opt})| \propto |\omega_{opt} - \omega_0|^N$ for even N and $|\hat{H}_{tx}(\omega_{opt})| \propto |\omega_{opt} - \omega_0|^{N-1}$ for odd N. In addition, the grating's central Bragg frequency should be designed to coincide with the signal's carrier frequency, i.e., ω_0. Notice that the LC-FBG reflection bandwidth,

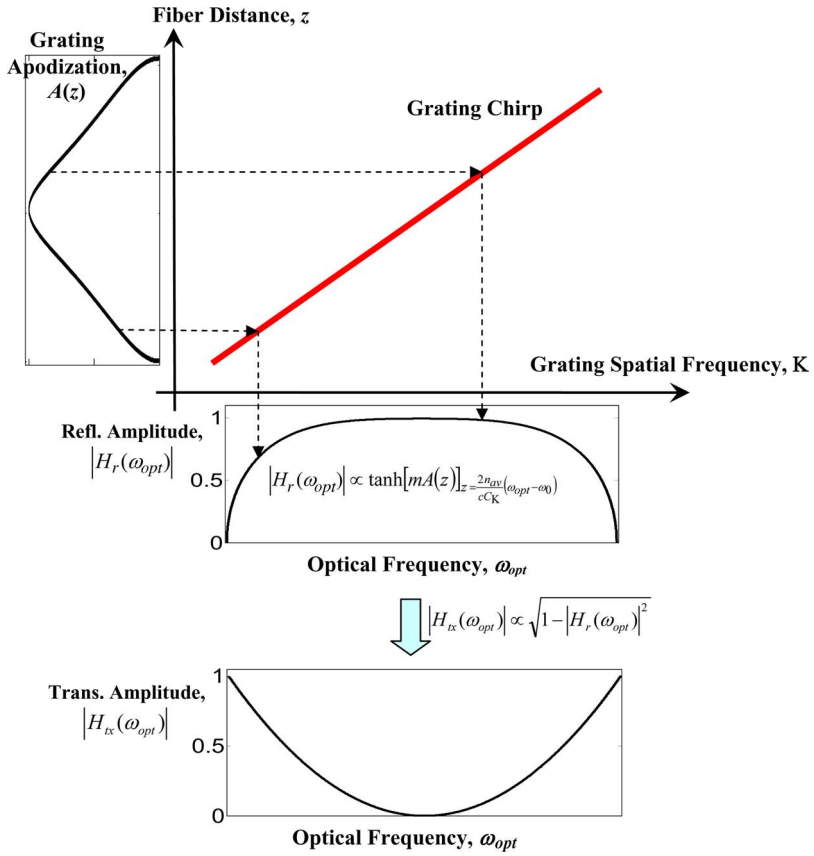

Fig. 6. Schematic illustration of the relationships between the physical grating parameters and the amplitude spectral responses of an especially apodized LC-FBG.

$\Delta\omega_R$, which determines the differentiator operational bandwidth (maximum processing speed), essentially depends on the grating chirp and length, i.e., $\Delta\omega_R \approx cC_K L/(2n_{av})$. Processing bandwidths at least in the subterahertz range can be achieved with practical LC-FBG devices [16].

The design equation (3) is strictly valid for low- to moderate-reflection FBGs [72]. However, in our devices, a reflectivity approaching 100% should be targeted at the resonance frequency (central Bragg frequency ω_0), where the grating transmission should be zero. Thus, whereas Eq. (3) allows us to obtain an accurate estimate of the grating apodization profile at points relatively far from the grating center $(z = 0)$, i.e., corresponding to the spectral regions sufficiently far from the resonance frequency, this equation cannot be used to design the grating apodization profile around $z = 0$, i.e., in the region corresponding to the close vicinity of the resonance frequency. In fact, the apodization profile resulting from Eq. (3) to approach a zero transmission should ideally tend to infinity at the center of the grating, which is a requirement that is physically impossible. Different methods can be employed to design the grating apodization profile around $z = 0$ so that to better approach the target spectral response in the vicinity of the resonance frequency; these include simple trial and error procedures, or the use of more systematic FBG synthesis tools (e.g., layer-peeling algorithms [58]). In any case, the grating transmission response obtained in a practical device will typically deviate from the ideal one in the spectral region around the resonance frequency; this translates into an increased processing error for longer input optical waveforms (a longer signal duration corresponds with a narrower frequency resolution) [16]. Hence, the transmission FBG approach for photonic differentiation is practically limited not only in terms of processing bandwidth (as for any practical filtering method) but also concerning the maximum time duration of the input optical waveform that can be processed with a prescribed accuracy.

2.2.2. Experimental results

LC-FBGs performing even-order operations were designed following the above strategy and were fabricated by the group of LaRochelle at the *Université Laval*, Quebec (Canada). Two examples of fiber-grating filters designed to perform second-order and fourth-order differentiation [25] are revisited here. The gratings were written in a CorActive UVS-INT fiber with a 244-nm frequency-doubled argon ion laser using the phase mask scanning method [56]. The chirp of the used phase mask was 0.5 nm/cm and the total length of each grating was 10 cm. The designed grating apodization profiles for the two target differentiation filters are shown in Fig. 7(a); the shown profiles are normalized with respect to the refractive index modulation peak $(\sim 6 \times 10^{-4})$ of the fourth-order device. The transmission spectral characteristics of the samples were measured using a commercial Optical Vector Analyzer (Luna Technologies), and they are shown in Fig. 7(b) and (c), together with the targeted spectral responses. An excellent agreement between the measured FBG responses and the spectral transfer functions of the corresponding ideal differentiator devices was achieved. The devices were successfully demonstrated for differentiation of picosecond optical pulses. For pulse characterization, we employed an SI setup similar to the one described above for the temporal testing experiments of the first-order differentiator [71]. The ultrashort Gaussian-like input pulses used in the different tests were generated from a passively mode-locked fiber laser (Pritel Inc.) at a repetition rate of $\sim$16.7 MHz. The pulses were spectrally centered at the central Bragg wavelength of the FBGs (minimum transmission wavelength), $\sim$1557.2 nm. The input pulse bandwidths were in the range from $\sim$125 GHz to $\sim$200 GHz (FWHM in intensity), depending on the specific measurement. Fig. 8 shows the experimentally recovered intensity and phase temporal profiles of the pulses obtained at the output of the tested differentiators, from second to fourth order. Notice that the second- and fourth-order differentiations were achieved by direct propagation of the input pulses through the corresponding LC-FBG device (i.e., devices with the spectral transmission responses in Fig. 7). For third-order differentiation, the second-order LC-FBG was concatenated with a first-order differentiator based on a full-coupling uniform LPG [25]; the used LPG was similar to the ones reported in Section 2.1.2 above but with a slightly narrower operational bandwidth, matching that of the FBG-based even-order differentiators. For all the temporal response tests, we observed an excellent agreement between the experimentally recovered time profiles and the ideal ones calculated through numerical differentiation (with the corresponding order) of the input ultrashort pulse waveform, which was in turn obtained by Fourier transformation of the measured input pulse spectral amplitude. The expected π phase shifts between the different time lobes in the output intensity profiles, corresponding to the predicted sign change in the numerical derivatives of the input pulse, were also accurately recovered. The energetic efficiency (defined as the output-to-input pulse energy ratio) for the pulse differentiation operations shown in Fig. 8 was estimated to be 1.4% (second order), 0.03% (third order), and 0.2% (fourth order). The energetic efficiency of the odd-order differentiator, which is based on the concatenation of two grating passive devices, is significantly lower than that of the single-device even-order differentiators. Notice also that the efficiency of the even-order devices typically decreases as the differentiation order is increased.

2.3. Brief Discussion on Applications of Ultrafast Photonic Differentiators

In analogy with their electronic counterparts [4], [5], photonic time differentiators are fundamental signal processing elements with a very wide range of potential applications. They are indeed considered as "basic building blocks" for constructing complex, multifunctional analog optical computing and information processing circuits devoted to a broad variety of applications [4]. The possibility of creating these circuits using photonic technologies translates into potential processing speeds orders of magnitude higher than those achievable with conventional electronic technologies. As discussed in the introduction, a relevant example of application of photonic differentiators is their use in ultrafast analog computing systems aimed at solving differential equations in real time at speeds well beyond the reach of present digital or analog computing platforms. Photonic differentiators are also of interest for ultrashort optical pulse shaping and ultrahigh-speed coding [7],

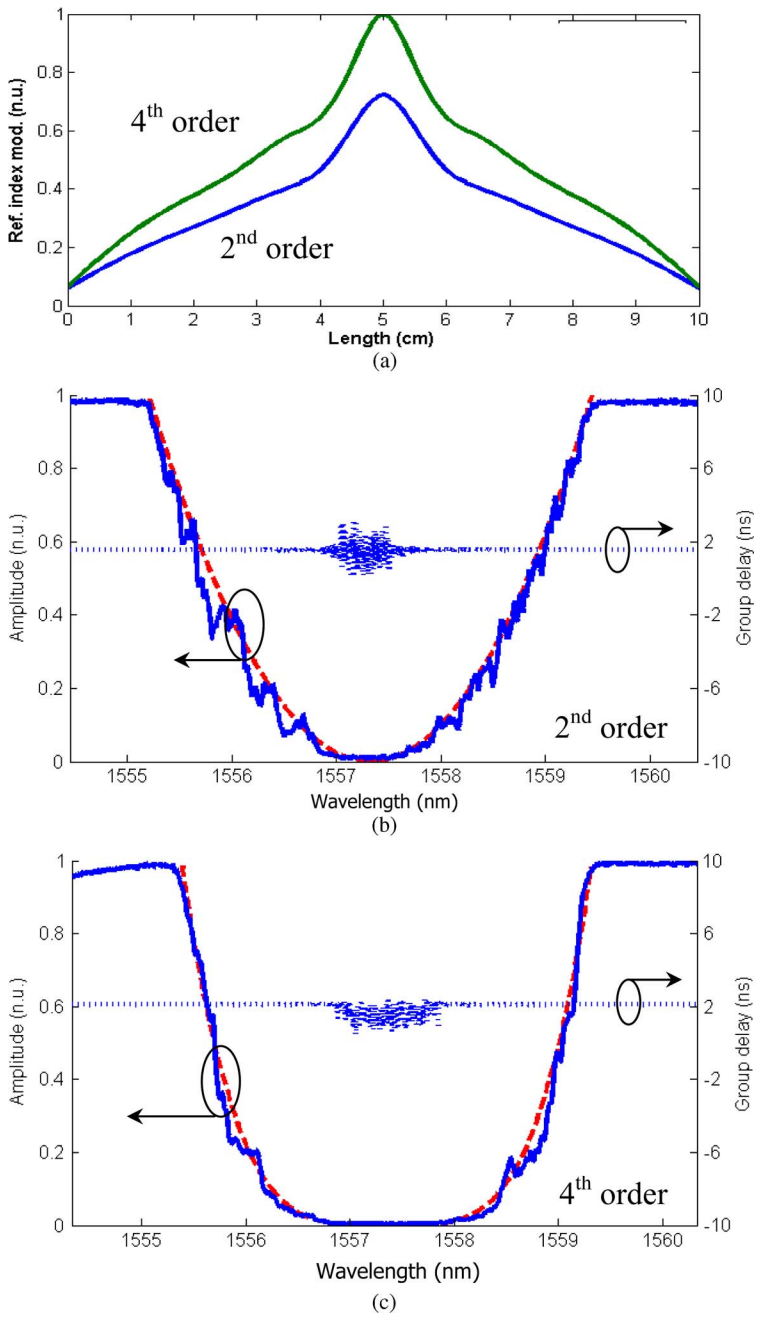

Fig. 7. (a) Normalized LC-FBG apodization profiles for second- and fourth-order photonic differentiators. Normalized measured spectral transmission response of the fabricated especially apodized LC-FBG devices for (b) second-order and (c) fourth-order photonic differentiation. The amplitude spectral transfer functions of the ideal differentiators are also shown (dashed curves) (from [25]).

[9], [10], [13], [60]–[62], ultrafast sensing and control [7], and for optical temporal waveform and device measurements [63]–[65]. A few of these applications are briefly discussed in what follows.

The fiber-grating differentiators discussed above were used for re-shaping sub-picosecond Gaussian-like optical pulses, as directly generated from a mode-locked laser, into their successive time derivatives, i.e., so-called temporal Hermite–Gaussian (HG) waveforms; see the results in Figs. 5 and 8 [9], [25]. Generating such odd-symmetry pulse waveforms in a relatively simple and efficient way poses challenges, since precise local changes in phase (exactly π) along the

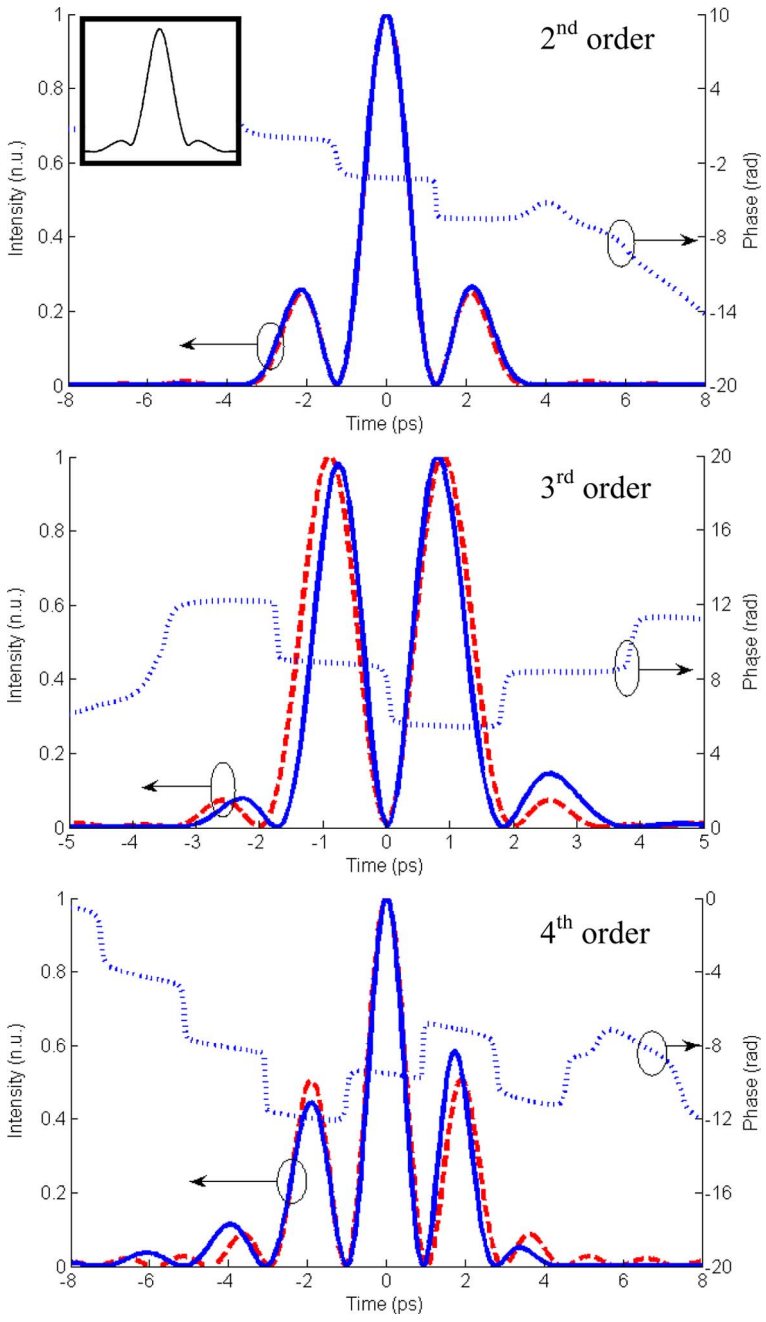

Fig. 8. Measured intensity (solid curves) and phase (dotted curves) temporal responses to a picosecond Gaussian-like input pulse of the demonstrated all-fiber second-, third-, and fourth-order photonic differentiators. For comparison, the numerically calculated successive time derivatives of the input optical pulse (presented in the inset using the same temporal scale) are also shown (dashed curves). (From [25]).

waveform duration are required. Subpicosecond HG waveforms were generated for the first time in optical fibers using the simple and efficient scheme described here, i.e., using propagation of the original Gaussian-like optical pulses through fiber-grating-based photonic differentiators. In particular, first-order (odd-symmetry) HG, OS-HG, pulse waveforms were generated by first-order differentiation of subpicosecond Gaussian optical pulses, see results in Fig. 5 [9]. This specific waveform is of interest for next-generation optical communications. The OS-HG waveform is a good approximation of the second-order dispersion-managed (DM) temporal soliton, also called a

soliton molecule" [73], [74]. A soliton molecule is the second solution of the nonlinear Schrödinger equation (the first solution is well approximated by a Gaussian waveform), which describes the pulse propagation in an optical fiber with periodically varying (positive and negative) dispersion. Since the first- and second-order DM solitons are temporally orthogonal and generally carry a different amount of energy, it has been suggested that the OS-HG waveform could be used as a new communication symbol in DM links, potentially leading to a considerable increase of the information capacity limit in fiber-optic communications systems [74].

Other potential applications for optical differentiators are related with the fact that the HG functions (including the original Gaussian pulse) constitute a *complete* set of orthogonal wave functions which can then be suitably combined to synthesize any desired temporal waveform [62]; said another way, any desired temporal pulse shape can be synthesized by properly combining the different successive time derivatives of a given input Gaussian-like optical pulse (including this pulse itself), generated using the simple optical differentiation devices discussed here, with specific relative weights. We have recently applied this general concept for reshaping Gaussian-like optical pulses into picosecond and subpicosecond flat-top (square-like) temporal intensity waveforms by simple propagation of the original pulses through an LPG-based first-order optical differentiator [61]; in this scheme, the pulse central frequency is properly detuned from the resonance frequency of the differentiator (zero-transmission frequency), which effectively results in the generation of a combination of the original pulse and its first time derivative, with relative weights determined by the pulse-LPG resonance frequency detuning. By properly fixing this frequency detuning, flat-top optical waveforms can be accurately synthesized at the LPG output. This simple strategy recently enabled the generation of the shortest flat-top waveforms ever synthesized using an all-fiber device, down to the subpicosecond range [61], i.e., around one order of magnitude shorter than with previous FBG-based pulse shapers [75]. It should be noted that flat-top temporal intensity profiles are highly desired for a range of nonlinear optical switching and frequency conversion applications [76], [77]; the ultrashort flat-top pulses generated from LPG integrators have been successfully employed to significantly improve the timing-jitter tolerance and general bit-error-rate performance of optical switching platforms in fiber-optic telecommunication links, i.e., optical time-division demultiplexing systems, operating at bit rates as high as 640 GHz [78].

Photonic temporal differentiators have also proved useful for full (amplitude and phase) characterization of optical waveforms [63]. Phase recovery methods from temporal intensity measurements have been developed by exploiting the fact that a photonic differentiator operates on the complex time profile of the input signal, including both its amplitude (intensity) and phase profiles. As a result, the time intensity waveform at the differentiator output depends on both the intensity and the phase temporal profiles of the input pulse. It has been demonstrated that the phase profile (both continuous and discrete-time phase variations) of a given optical waveform can be recovered from measurements of the temporal intensity profiles of the signal under test before and after propagation through a first-order photonic differentiator, e.g., uniform LPG [63]. This simple technique has proved particularly useful for accurate characterization of the group delay and phase spectral responses of dispersive devices, e.g., LC-FBGs, using a conventional time-domain intensity measurement setup [65]. By use of a previously characterized fiber dispersive device combined with an ultrafast first-order photonic differentiator, accurate measurements of pulse waveforms with durations ranging from a few picoseconds to tens of nanoseconds and submilliwatt average powers have been experimentally achieved [64].

3. Ultrafast Photonic Temporal Integrators

3.1. First-Order Photonic Integrators Based on Uniform FBGs

3.1.1. Operation principle

A first-order photonic temporal integrator is a device that "calculates" the first time cumulative integral of the complex envelope of an incoming arbitrary optical waveform (see Fig. 9),

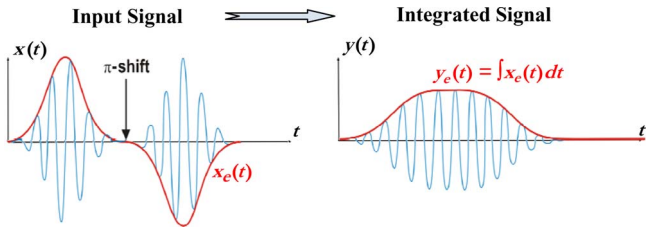

Fig. 9. Operation of an ideal photonic integrator on an input arbitrary optical signal.

mathematically $y_e(t) \propto Int\{x_e(t)\} = \int x_e(t)dt = \int_{-\infty}^{t} x_e(t')dt'$, where *Int* is the integral operator, and $x_e(t)$ and $y_e(t)$ are the complex temporal envelopes of the input and output optical signals, both spectrally centered at the same optical frequency, ω_0 (carrier frequency).

It can be easily demonstrated that the above cumulative integral can be mathematically expressed as follows:

$$Int\{x_e(t)\} \propto \int_{t'=-\infty}^{t} x_e(t')dt' = \int_{\tau=0}^{+\infty} x_e(t-\tau)d\tau = \int_{\tau=-\infty}^{+\infty} u(\tau)x_e(t-\tau)d\tau \tag{4}$$

where the second integral has been obtained by introducing a simple variable change, $t' = (t-\tau)$, and $u(t)$ is the so-called unit step function

$$u(t) = \begin{cases} 1, & t \geq 0 \\ 0, & t < 0. \end{cases}$$

The last integral in Eq. (4) represents a convolution between the input time envelope $x_e(t)$ and the unit step function $u(t)$ [4]. This implies that the desired time integral can be obtained by simply processing the input signal with a linear time-invariant optical system (i.e., optical filter) providing a temporal impulse response (filter's response to a temporal impulse $\delta(t)$ launched at the reference time $t = 0$) with an envelope proportional to the unit step function, $u(t)$, and spectrally centered at the signal's carrier frequency ω_0. Notice that the unit step function ideally extends to infinity and consequently, a filter having a temporal impulse response proportional to this ideal infinite-duration function should necessarily require the use of a gain mechanism (i.e., an active device); this would indeed translate into some important drawbacks such as a high noise level (originating from spontaneous emission from the employed gain medium), high energy consumption, and additional technical challenges for fabrication and operation of the device. Fortunately, it is known from electronics that the ideal impulse response of a temporal integrator can be "emulated" within certain limits using passive filtering architectures [6], thus avoiding the use of active filtering devices.

The solution described here for first-order photonic integration [36] is based on the use of a passive linear optical filter providing a temporal impulse response that emulates the ideal one (unit step function) over a finite time duration, T_h; said another way, the idea is to use a passive optical filter with a square temporal impulse response envelope; mathematically

$$h_{e,1}(t) \propto \begin{cases} 1, & 0 \leq t \leq T_h \\ 0, & \text{otherwise.} \end{cases} \tag{5}$$

It can be easily anticipated that a filter with such an impulse response should be able to "calculate" the time integral of an arbitrary input signal over a time duration equal to the impulse response time-width T_h; this is usually referred to as the operational time window of the passive

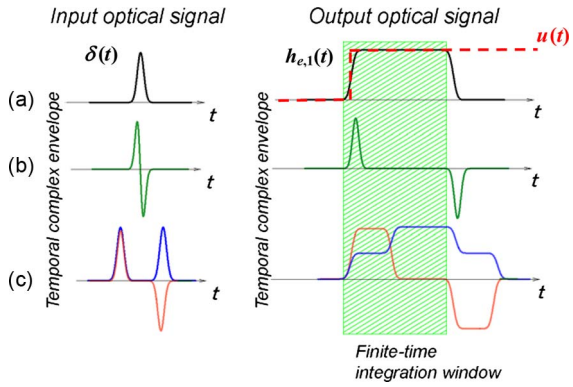

Fig. 10. Theoretical input (left) and output (right) pulses from a finite-time photonic integrator (square-like impulse response) for different input waveforms. (a) Gaussian ultrashort pulse. (b) OS-HG pulse, i.e., first time derivative of a Gaussian pulse. (c) Symmetric and odd-symmetry double pulses. The plots in (a) also serve to illustrate the response to the temporal impulse $\delta(t)$ of a finite-time integrator, i.e., square-like function $h_{e,1}(t)$ shown with a black, solid curve, as a time-limited approximation of the impulse response of an ideal (infinite-time) integrator, i.e., unit-step function $u(t)$ shown with a red, dashed line. (From [39]).

integrator. To be more concrete, the square time waveform in Eq. (5) can be expressed as a function of the temporal impulse response of an ideal integrator (unit step) as follows:

$$h_{e,1}(t) \propto u(t) - u(t - T_h). \tag{6}$$

Thus, the signal obtained at the output of this filter when a waveform $x_e(t)$ is launched at its input is given by the following:

$$y_e(t) \propto \int_{\tau=-\infty}^{+\infty} h_{e,1}(\tau) x_e(t-\tau) d\tau = Int\{x_e(t)\} - Int\{x_e(t - T_h)\}. \tag{7}$$

Hence, as anticipated, a passive optical filter with a square-like temporal impulse response of duration T_h, such as that defined by Eq. (5), produces a temporal waveform at its output that follows the profile of the integral of the input waveform over a finite time window of duration T_h; a second delayed integral pattern is subtracted to the main one after the operational time window, leading to a distortion of the desired integral profile. Thus, the signal integral will be accurately recovered over a limited time window which can be designed to exceed the duration of the input signal waveform. If necessary, an additional temporal modulation mechanism may be used to extract the valid integrated signal (extending over an interval of duration T_h) from the full temporal pattern. Possible practical implementations include electro-optic pulse pickers or nonlinear optical switchers. Relevant examples of signal processing operations based on the use of a finite-time photonic integrator with a square-like impulse response are illustrated in Fig. 10. Concerning the double-pulse waveforms [see Fig. 10(c)], the integrator will simply sum up the area under the two pulses in time when the two pulses are in phase, resulting in two consecutive steps, respectively, corresponding to the integration of the leading pulse and the subsequently added integration of the trailing pulse. In contrast, when the two input consecutive pulses are out of phase, the second optical pulse will compensate for the cumulative time integral of the first pulse, leading to a square-like (flat-top) output time profile with a duration fixed by the input interpulse delay.

A filter with a square-like temporal impulse response such as that defined in Eq. (5) will have a spectral transfer function determined by the Fourier transform of this impulse response, namely, the

well-known sync function [4]

$$\hat{H}_1(\omega_{opt}) \propto \frac{\sin(\omega T_h/2)}{\omega} \exp(j\omega T_h/2) \tag{8}$$

where $\omega = \omega_{opt} - \omega_0$. We recall that for accurate processing, the input signal should be spectrally centered at the filter's central frequency, ω_0. The spectral transfer function in Eq. (8) should be contrasted with that of an ideal photonic integrator [4], $\hat{H}_{1,ideal}(\omega_{opt}) \propto 1/(\omega_{opt} - \omega_0)$. As expected, while the spectral response of a finite-time integrator can be implemented using a passive filtering device (the transfer function in Eq. (8) should be simply normalized to a maximum of 1), the same is not true for an ideal, infinite-time, integrator: The spectral response of an ideal integrator is necessarily higher than 1 in the vicinity of ω_0, ideally diverging to infinity at ω_0 (i.e., the ideal filter should have a pole at its central frequency). This ideal functionality can be fully approached only by use of an active filtering mechanism. One can easily prove that the spectral transfer function in Eq. (8) can be also inferred from the expression of the corresponding impulse response in Eq. (6) as a function of the responses of two time-delayed ideal integrators. Thus, the combination of these two time-delayed ideal integration operations (each with an associated frequency response having a central pole) translates into a purely passive frequency response (with no poles).

A very interesting finding is that the square-like temporal impulse response of a time-limited integrator is intrinsically provided by a weak-coupling (low reflectivity) uniform FBG operated in reflection [72], [79]. An FBG operates in the weak-coupling regime when $\kappa L \ll \pi$, where κ is the grating coupling coefficient per unit length, and L is the total FBG length; in practice, this condition typically implies that the peak reflectivity of the FBG keeps lower than $\sim$10%. It is very well known that the reflection temporal impulse response of a weak-coupling uniform FBG is approximately constant (square-like) over a finite time duration fixed by the round-trip propagation time along the grating length, i.e., $T_h \approx 2n_{av}L/c$ [79]. This is so because an ultrashort time impulse propagating through a FBG is reflected at each local position as it propagates through the grating, generating a reflected signal at the corresponding round-trip time. In the case of a weak-coupling grating, only a small fraction of the input pulse energy is reflected at each position in such a way that (considering a FBG with a uniform coupling strength along its length) the amount of reflected energy is nearly identical at any reflection location along the grating length; the input impulse propagates all the way to the end of the FBG and keeps interacting with it, continually generating a reflected signal with a nearly constant reflection magnitude. Currently, high-quality uniform FBGs with lengths above 10 cm, corresponding to round-trip propagation times (operational integration times) above 1 ns, can be routinely fabricated. The device's processing speed will be limited by the frequency bandwidth over which the filter can resemble the ideal sync spectral transfer function in Eq. (8). In a practical FBG, this is limited by the finite spatial resolution of the photo-inscribed fiber-grating profile: An improved grating spatial resolution translates into a uniform refractive-index profile with steeper edges and an associated larger operational bandwidth. Grating bandwidths approaching the terahertz range are feasible (corresponding to spatial resolutions < 100 μm) [56]. However, in practice, the maximum signal bandwidth that can be processed will be ultimately limited by energetic considerations [39]. For a given FBG integrator, the broader the input signal bandwidth the poorer the energetic efficiency of the integration process will be (a larger portion of the input pulse energy will be filtered out). In this respect, the uniform FBG solution [36] still represents a relatively efficient design, particularly as compared with alternative FBG passive integrator designs [38] for which the input signal bandwidth must necessarily be much broader than the grating reflection bandwidth.

3.1.2. Experimental results

A weak-coupling 5-mm-long uniform FBG sample, which was fabricated by the group of Yao at the *University of Ottawa* (Canada), was used for our experimental demonstrations [39]. The grating physical length corresponds to an integration time window of $\sim$50 ps. The FBG was written using a

frequency-doubled argon-ion laser operating at 224 nm with a uniform phase mask having a period of 1071 nm. Operation in the weak-coupling regime was ensured by keeping the FBG peak reflectivity lower than 10%, which was achieved by control of the UV exposure time during the fabrication process [56]. For operation as a photonic integrator, the FBG needs to be operated in reflection, which requires the use of an additional device, e.g., optical circulator, to retrieve the reflected signal. In our experimental demonstrations, a passively mode-locked tunable fiber laser (Pritel Inc.) was used as the input pulse source, which generated nearly transform-limited Gaussian-like optical pulses, each with a FWHM time duration of $\sim$6 ps, at a repetition rate of 16.7 MHz. Notice that the FBG was mounted on a fiber holder and a weak axial strain was applied to the FBG with the aim of adjusting the resonance wavelength to coincide with the carrier wavelength of the input optical signal in each experiment.

The Gaussian-like pulse directly generated from the fiber laser was reshaped into various different waveforms using an optical pulse shaper based on a single two-arm (Michelson) bulk-optic interferometer [13], [80]. These properly reshaped waveforms were used as the input optical signals in the tested FBG integrator. For generating an OS-HG waveform from the input Gaussian-like optical pulse, a temporal differentiation process was implemented [13]; for this purpose, the interarm relative delay in the Michelson interferometer was fixed to achieve a destructive spectral interference at the center wavelength of the input Gaussian-like pulse. In this case, the spectral transfer function of the interferometer approximates the spectral response of an ideal differentiator over a bandwidth of about 30% of the spectral period between destructive interferences (i.e., 30% of the interferometer's FSR) [13]; thus, the relative delay in the interferometer was adjusted to ensure that the resulting differentiation band coincided with the full spectral bandwidth of the input pulse. Concerning the double-pulse generation, the interferometer's FSR was adjusted to be narrower than the input pulse spectral bandwidth so that the pulse replicas in time were separated. (We are reminded that the interferometer's FSR is inversely proportional to the relative time delay between the interferometer arms). In-phase pulse replicas were achieved by tuning the interferometer's constructive interference to be centered at the pulse carrier wavelength, whereas out-of-phase replicas were obtained by tuning the interferometer's destructive interference to be centered at the pulse carrier wavelength.

For full (amplitude and phase) time-domain characterization of the ultrafast pulse waveforms, we used an SI setup similar to that employed for the time-domain testing experiments of optical differentiators [71]. Fig. 11(a)–(d) show the measured temporal complex envelopes of the input and output optical signals in some of the performed experiments. The results in Fig. 11(a) are for the integration experiment of an OS-HG pulse. This pulse was obtained by first-order time differentiation of the input Gaussian-like pulse (laser pulse) using the Michelson interferometer [13]. The generated OS-HG waveform, as in Fig. 11(a)-i, consisted of two π-phase shifted consecutive temporal lobes, each with an individual FWHM time width of $\sim$7.5 ps, temporally separated by $\sim$21.8 ps. As expected, the reflected waveform from the FBG, as in Fig. 11(a)-o, over the integration time window (marked with a gray box), was a nearly transform-limited (constant-phase) Gaussian-like pulse, almost identical to the original laser pulse, in good agreement with the theoretical predictions in Fig. 10(b). The experimentally measured temporal pulse profile agrees very well with the numerical time integral (shown with red hollow circles) of the measured input OS-HG pulse waveform.

The results shown in Fig. 11(b) and (c) correspond to integration of two odd-symmetry double-pulse waveforms, each consisting of two π phase-shifted replicas of the 6-ps (FWHM) input laser pulse, with different time separations (28.3 ps and 35.9 ps). The reconstructed temporal waveforms at the FBG integrator output are shown in Fig. 11(b)-o and Fig. 11(c)-o, respectively, showing again an excellent agreement both with the numerical integrations of the corresponding measured input pulse waveforms (over the indicated integration time window) and with the theoretical predictions in Fig. 10(c). As expected, flat-top optical pulses were generated over the integration time window, each with a different FWHM time duration, as fixed by the time separation between the input odd-symmetry twin pulses. Finally, we also tested the integration of a symmetric double-pulse structure, consisting of two in-phase replicas of the 6-ps input laser pulse temporally separated by $\sim$30.5 ps,

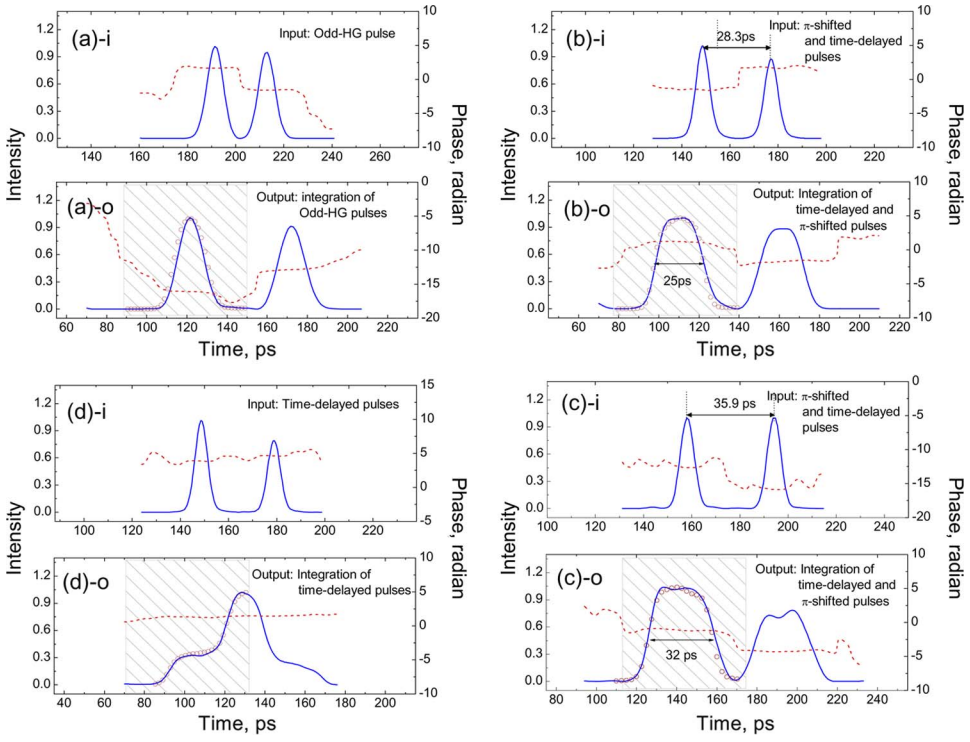

Fig. 11. Experimentally measured input and output temporal waveforms for different integration experiments. (a) Integration of an OS-HG input pulse, (b), (c) integration of odd-symmetry double-pulse waveforms with different input interpulse delays, and (d) integration of a symmetric double pulse. In each plot, the top subplot (named by the suffix "-i") shows the signal launched at the input of the FBG (integrator), whereas the bottom subplot (named by the suffix "-o") shows the signal reflected from the FBG (integrator output), illustrating the integration time window with a gray box and presenting the theoretical (numerical) time integral of the measured input complex envelope along the integration window (curve with red hollow circles). In each subplot, the measured temporal intensity profile is represented with a solid blue line, and the measured temporal phase profile is represented with a dashed red line (from [39]).

as shown in Fig. 11(d). The obtained temporal pulse profile is in excellent agreement both with the finite-time numerical integration of the measured input waveform and with the theoretically predicted temporal profile in Fig. 10(c). The reported results clearly confirm that the developed FBG-based integrator operates on the *complex* envelope (amplitude and phase) of the incoming optical waveforms.

The energetic efficiencies of the reported integration examples, i.e., integrations of an OS-HG, an odd-symmetry double pulse and a symmetric double pulse, (defined by the ratio of the output time-average power to the input time-average power) were measured to be 0.3%, 0.4%, and 1.1%, respectively. This low energy efficiency is due to the fact that the integration signal is reflected from a weak-coupling FBG. Moreover, as discussed above, the energetic efficiency of the integration process is degraded when processing an optical signal with a broader spectral bandwidth, which practically limits the maximum signal bandwidth that can be processed with a FBG of a given length.

3.2. Optimized Arbitrary-Order Photonic Integrators Based on FBGs

3.2.1. Operation principle and FBG design

An *N*th-order photonic integrator $(N = 1, 2, 3, \ldots)$ is a device that provides the *N*th time integral of the time complex envelope of an input arbitrary optical waveform. The output from an *N*th-order

photonic integrator when an optical signal of complex envelope $x_e(t)$ is launched at its input has a temporal envelope given by

$$y_e(t) \propto \int_{\tau_N=-\infty}^{t} \dots \int_{\tau_1=-\infty}^{\tau_2} x_e(\tau_1) d\tau_1, \dots, d\tau_N. \tag{9}$$

Following a similar derivation to that detailed above for a first-order integrator, this general functionality can be implemented using a linear optical filter centered at ω_0 (carrier frequency of the input and output optical signals) and with a temporal impulse response envelope defined by the following expression:

$$h_{e,N}^{ideal}(t) \propto \int_{\tau_N=-\infty}^{t} \dots \int_{\tau_1=-\infty}^{\tau_2} \delta(\tau_1) d\tau_1, \dots, d\tau_N = \frac{t^{N-1}}{(N-1)!} u(t) \tag{10}$$

where we recall that $u(t)$ is the unit-step function. The ideal impulse response derived in Eq. (10) extends to infinity, thus requiring the use of a linear optical filter incorporating a gain mechanism. Similarly to the above detailed strategy for a first-order integrator, our proposed design approach is based on the use of a *passive* linear optical filter that emulates the ideal temporal impulse response in Eq. (10), i.e., with amplitude proportional to t^{N-1}, over a finite time window, namely, over the interval $0 \leq t \leq T_h$ [37]

$$h_{e,N}(t) \propto t^{N-1} \prod\left(\frac{t - T_h/2}{T_h}\right) \tag{11}$$

where the function $\prod((t - T_h/2)/T_h)$ is the square function of duration T_h, centered at $T_h/2$, i.e., this is a constant in the interval $0 \leq t \leq T_h$ and zero elsewhere. This passive filter provides the Nth-order time integral of an arbitrary incoming optical waveform over a finite time window of duration T_h, extending from the integral's starting time. Notice that the output signal is not necessarily zero outside the integration time window, even when the impulse response is forced to be zero outside this window. If necessary, an additional temporal modulation mechanism may be used to extract the valid integrated signal (extending over an interval of duration T_h) from the full temporal pattern.

The required temporal impulse response for a time-limited arbitrary-order optical integrator, as defined by Eq. (11), can be implemented using a simple weak-coupling uniform-period FBG with a proper grating apodization profile [37]. An FBG strictly operates in the weak-coupling regime when its peak reflectivity is lower than ~10%. In this case, the reflection temporal impulse response envelope, $h(t)$, is approximately proportional to the grating apodization profile $A(z)$ (variation of the refractive-index modulation) after the suitable space-to-time scaling [72]. Mathematically, $A(z) \propto h(t = 2n_{av}z/c)$, for $0 \leq z \leq L$ ($0 \leq t \leq 2n_{av}L/c$), where we recall that n_{av} is the average refractive index of the uniform-period FBG, c is the speed of light in a vacuum, and L is the total grating length. Thus, in order to achieve Nth-order integration over a time window of duration T_h, the FBG should provide a temporal impulse response $h(t) = h_{e,N}(t) \propto t^{N-1}$ along the interval $0 \leq t \leq T_h$ and as a result, the grating apodization profile should vary proportionally to the $(N-1)$ power of the grating length, i.e., $\Delta n(z) \propto z^{N-1}$ over the fiber length $0 \leq z \leq z_h$, with $z_h = cT_h/2n_{av}$ [37]. Notice that the solution discussed above for first-order integration can be simply interpreted as a particular case of this general design approach (for $N = 1$).

As a main drawback, the resulting FBG filters from this general design approach are necessarily low reflectivity, which adversely affects the energetic efficiency of the integration process. This actually represents one of the fundamental drawbacks of weak-coupling FBG integrators, limiting, for instance, the maximum bandwidth (processing speed) of the input signals that can be accurately and efficiently processed. The filters' energetic efficiency can be significantly improved by designing

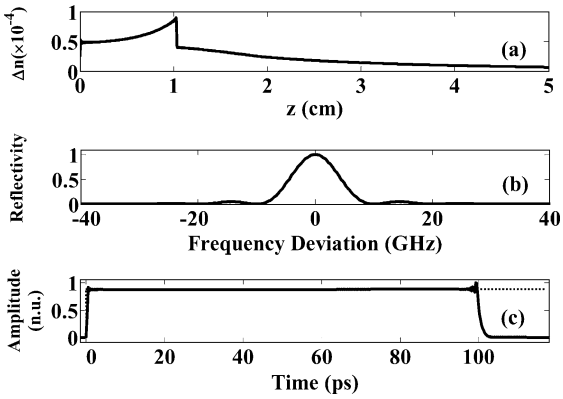

Fig. 12. Spectral and temporal impulse responses of a first-order optical integrator based on a 5-cm-long uniform-period FBG with the apodization profile plotted in (a). (b) Reflectivity as a function of frequency deviation (around 193 THz). (c) Amplitude of the reflection temporal impulse response (solid curve), shown in normalized units [n.u.]. The impulse response amplitude of an ideal first-order integrator is also shown (dotted curve) (from [40]).

high-reflectivity gratings providing the desired finite-time impulse responses, as defined by Eq. (11), e.g., using conventional FBG inverse scattering synthesis algorithms [58]. Whereas, in principle, one can anticipate that this may require the realization of more complex grating apodization and/or chirp profiles, it has been recently demonstrated [40] that if the grating is designed to be sufficiently long, then the needed apodization profile will be extremely simple, regardless of the integration order; specifically, a relatively smooth *amplitude-only* coupling-strength variation is required and no grating period chirping or discrete phase shifts need to be introduced in the FBG profile. The required grating apodization can be practically realized using an amplitude apodization mask or by properly controlling the UV exposure time along the fiber length [56].

3.2.2. Numerical results

For all of the designs presented here [40] an integration time window of $T_h = 100$ ps is targeted. We first designed a FBG with an impulse response given by Eq. (11) with $N = 1$ [i.e., impulse response in Eq. (5)], for first-order differentiation, and with a nearly 100% grating peak reflectivity. A layer-peeling synthesis algorithm [58] was used for this purpose. The application of the layer-peeling synthesis algorithm provided a solution for the required grating profile with no chirp (uniform-period) and with the amplitude-only apodization profile shown in Fig. 12(a). Fig. 12(b) presents the reflectivity—square magnitude of the grating's reflection spectral response as a function of the frequency deviation around $\omega_0 = 2\pi \times 193$ THz—of the designed FBG, confirming that we achieved the desired high peak reflectivity. Notice also that the FBG reflection spectrum exhibits the expected sync shape, as defined in Eq. (8). The amplitude of the FBG reflection temporal impulse response, calculated as the inverse Fourier transform of the FBG complex reflection spectral response, is shown in Fig. 12(c) (solid curve). For comparison, the impulse response of an ideal first-order integrator, i.e., the unit-step function, is also shown in Fig. 12(c) (dotted curve). The device's temporal impulse response exhibited the targeted square-like shape over the finite time window of duration $T_h \sim 100$ ps.

To confirm the operation of the designed first-order FBG integrator, we simulated the temporal response of this grating to various input optical waveforms. In the example presented here, the input waveform was the numerically calculated second time derivative of a transform-limited Gaussian optical with a FWHM duration of 10 ps (centered at $\omega_0 = 2\pi \times 193$ THz). The normalized temporal complex envelope of this input signal is shown in Fig. 13(a). Fig. 13(b) (black curve) shows the normalized temporal envelope of the waveform obtained after reflection from the designed first-order temporal integrator. For comparison, the output from an ideal first-order integrator (first time derivative of the defined Gaussian pulse) is also plotted with red circles in

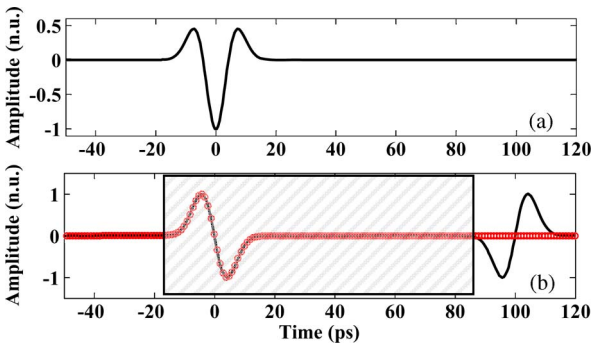

Fig. 13. Results from numerical simulations (all the plots show the complex envelopes in normalized units [n.u.]) for the FBG first-order integrator. (a) Optical waveform launched at the devices' input (second time derivative of a 10-ps Gaussian). (b) Optical waveform reflected from the FBG (black, solid curve) and ideal first-order integration of the input pulse, i.e., first time derivative of a 10-ps Gaussian (red circles). The operational time window of the integrator is indicated with a gray hatched box (from [40]).

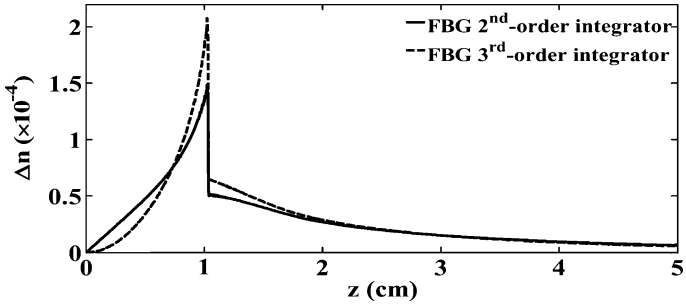

Fig. 14. Grating apodization profiles of the designed 5-cm-long FBG second-order and third-order optical integrators (from [40]).

Fig. 13(b). The simulated reflected waveform was almost indistinguishable from the corresponding ideal output waveform in the integration time window of $T_h = 100$ ps, which is indicated with a gray hatched box. Notice that for illustration purposes the time reference $(t = 0)$ of the input and output signals has been fixed to coincide with the center of the relevant waveform. As discussed above, the output from a finite-time temporal integrator is not necessarily zero outside the integration time window. In this specific case, a "mirrored" version of the integrated waveform was obtained outside the integration time window.

The results corresponding to FBG designs for second- and third-order temporal integrations are shown in Figs. 14–16. We have used the temporal impulse responses given by Eq. (11) for $N = 2$ and 3, with a maximum peak reflectivity approaching 100%, as the targeted grating reflection responses in the layer-peeling synthesis algorithm. The synthesized amplitude-only apodization grating profiles for the second- and third-order temporal integrators are shown in Fig. 14 with solid and dashed lines, respectively.

The amplitude of the temporal impulse response of the designed FBG second- and third-order temporal integrators are plotted in Figs. 15(a) and (b) (solid curves), respectively. For comparison purposes, the temporal impulse responses of the corresponding ideal integrators are plotted with dashed lines in the same figures. The spectral reflectivity of each FBG integrator is also plotted in the inset of the corresponding figure. Eq. (11) indicates that the temporal impulse response of a second-order integrator $(N = 2)$ should have a linear variation with time, whereas the impulse response of a third-order temporal integrator $(N = 3)$ should exhibit a quadratic dependence on the time variable along the integration time window. The impulse responses of the designed FBG second-order and third-order integrators exhibited very nearly the targeted theoretical profiles over

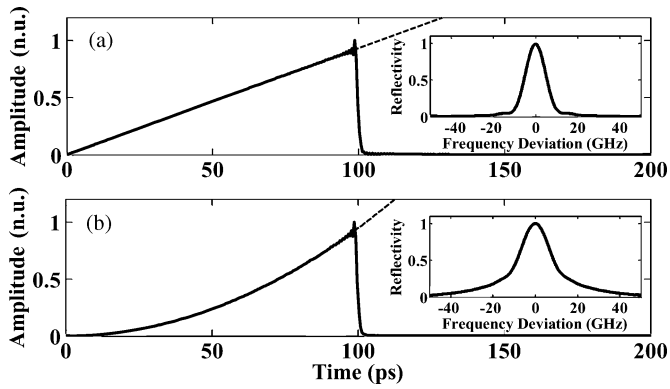

Fig. 15. Temporal impulse responses of (a) a second-order and (b) a third-order optical integrator, each based on a 5-cm-long FBG with the corresponding apodization profile plotted in Fig. 14. The impulse response amplitude of the corresponding ideal integrator is also shown in each plot (dotted curve). The inset of each plot shows the corresponding grating reflectivity as a function of frequency deviation (around 193 THz) (from [40]).

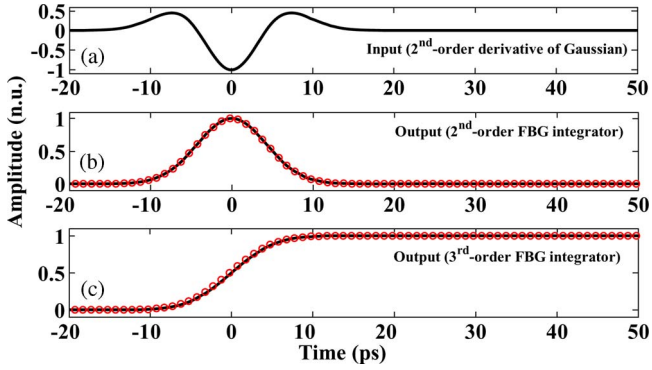

Fig. 16. Results from numerical simulations (all the plots show the complex envelopes in normalized units [n.u.]) for second- and third-order integrators [input is shown in (a)]. (b) Optical waveform reflected from the FBG-based second-order integrator (black, solid curve) and ideal second-order integration of the input pulse, i.e., a 10-ps Gaussian (red circles). (c) Optical waveform reflected from the FBG-based third-order integrator (black, solid curve) and ideal third-order integration of the input pulse, i.e., the integral of a 10-ps Gaussian (red circles) (from [40]).

a finite window of duration $T_h \sim 100$ ps while achieving a peak reflectivity of nearly 100% from each of these gratings. The operation of the designed gratings as second-and third-order optical integrators was confirmed by simulating the temporal responses of these gratings to various input optical waveforms. In the example presented here, the input waveform was the same input as that used for the FBG first-order integrator, replotted in Fig. 16(a). Fig. 16(b) and (c) (solid black curves) show the normalized and shifted-to-the-origin temporal envelopes of the waveforms obtained after reflection from the designed second- and third-order integrators, respectively. For comparison, the outputs from an ideal second-order integrator (the defined Gaussian pulse) and from an ideal third-order integrator (integral of the Gaussian pulse) are also plotted with red circles in Fig. 16(b) and (c), respectively. In both cases, the simulated reflected waveforms were almost indistinguishable from the corresponding ideal integrated waveforms over the predefined integration temporal window.

The passive FBG design described above for optimized arbitrary-order temporal integration of ultrafast optical waveforms has been experimentally demonstrated very recently [43]. Both first- and second-order ultrafast photonic integrators have been fabricated and tested, successfully proving

their capability for accurately and efficiently processing arbitrary optical waveforms with picosecond time features over an operation time window of ~60 ps. The demonstrated first-order passive temporal integrator offers an energetic-efficiency improvement of more than one order of magnitude, as compared with the weak-coupling uniform FBG-based device discussed in the previous section.

3.3. Brief Discussion on Applications of Ultrafast Photonic Integrators

Temporal integration is the signal processing counterpart of temporal differentiation. As discussed in Section 3.2, photonic differentiators have already been demonstrated for a wide range of applications in ultrafast optical pulse processing and shaping, photonic signal and device characterization, and optical control and sensing, among others. Applications in a similar range of fields can be anticipated for the photonic temporal integrator developed here. For instance, the proof-of-concept experiments presented above suggest various interesting specific applications for the realized photonic integrator, including reconfigurable flat-top pulse generation and phase-encoded pulse pattern recognition. The generation of ultrashort flat-top temporal intensity profiles is highly desired for a range of nonlinear optical switching and frequency conversion applications [76]–[78]. In these applications, the flat-top pulse time width needs to be optimized according to the features (e.g., bit rate) of the transmission link. None of the available all-fiber designs for flat-top pulse synthesis [61], [75] allows for pulse time-width tuning. A very simple mechanism for reconfigurable flat-top pulse generation based on the integration property of a uniform FBG has been demonstrated above, see results in Fig. 11(b) and (c). In particular, a flat-top optical pulse can be generated by simple reflection of an odd-symmetry double-pulse waveform in a uniform FBG; the flat-top width can be easily reconfigured by simply tuning the time separation between the input twin pulses. Concerning the second mentioned application, in view of the behavior described in Fig. 10(c) and the corresponding experimental demonstrations in Fig. 11(b)–(d), it is obvious that the integrator response (output intensity profile) to a sequence of consecutive input pulses depend on the discrete phase shifts among these pulses, thus suggesting a direct and simple mechanism for recovering the phase keys encrypted in a sequence of intensity bits.

A photonic integrator can be interpreted as the light-wave equivalent of an electronic capacitor [34]. As such, a photonic integrator is intrinsically an element capable of storing "photons". Loadable and erasable optical memory units with ultrafast switching times have been proposed based on photonic temporal integrators [35], [41], [66]. A particularly simple idea for a 1-bit memory unit is based on exploiting the results of integration of antisymmetric double pulses [66], see Fig. 10(c): In particular, the integrator-based memory could be loaded—i.e., switched to the state "1"—by launching an input "set" ultrashort pulse, and subsequently erased, or reset, to the state "0" by a pulse π-phase-shifted with respect to the "set" pulse. Memory switching times, fixed by the integrator processing speed, in the picosecond range together with memory life-times, determined by the integrator operational time window, in the nanosecond regime could be achieved using the simple FBG-based integrators described above.

Finally, we emphasize again the key use of photonic temporal integrators for implementing all-optical computing systems aimed at real-time solving of scientific and engineering problems that can be described by differential equations. In this context, it should be noted that whenever possible the use of integrators should be preferred to differentiators because the latter have a significantly worse performance in terms of high-frequency noise: A differentiator essentially amplifies the high-frequency noise that is present in the input signal to be processed while an integrator, which is essentially a low-pass filter, tends to reduce or eliminate this critical noise contribution.

4. Conclusion

In conclusion, this paper reviews recent work on the design, experimental implementation, testing, and applications of two fundamental analog signal processing elements, namely, time differentiators and integrators, implemented in the all-optical domain, with a particular emphasis

on fiber-grating-based solutions. It has been shown that the simplest fiber-grating devices, namely a uniform LPG and a uniform FBG, can be designed to implement a first-order ultrafast all-optical differentiator and a first-order ultrafast all-optical integrator, respectively. These fundamental findings have established the basis to design photonic differentiators and integrators with improved features (e.g., enabling high-order operations or with improved performances) based on relatively more complicated LPG and FBG devices. Photonic differentiators and integrators offering processing speeds up to the terahertz range have been experimentally implemented and successfully tested.

These basic all-optical signal-processing devices have been also demonstrated for a wide range of applications, including (sub)picosecond pulse shaping for ultrafast coding and switching operations in fiber-optic telecommunications, measurement of ultrafast pulse waveforms, characterization of photonic devices and systems, and implementation of optical memory units. Other suggested applications for photonic differentiators and integrators include ultrafast analog computing systems aimed at solving differential equations and sensing and control units. For some of these applications, the implementation of photonic differentiators and integrators in monolithic platforms, fully compatible with future integrated photonic circuits, would be highly desired. Additionally, the fiber-grating concepts in which the all-optical processors discussed here rely upon could be potentially transferred to integrated-optic platforms.

Acknowledgment

The author would like to thank one of the anonymous referees for very insightful input into some of the concepts discussed in the paper, as well as for pointing out some relevant references. The work reviewed in this paper has involved numerous contributions from colleagues at INRS and other research institutions. I am particularly indebted to the following persons: Y. Park, M. H. Asghari, L.-M. Rivas Asensio, K. Singh, and F. Li (INRS), R. Slavík (Southampton University, U.K., on leave from the Academy of Sciences of the Czech Republic), M. Kulishov (HTA Photomask Inc., San Jose, CA), S. Boudreau and S. LaRochelle (Université Laval, Quebec, QC, Canada), Y. Dai and J. Yao (University of Ottawa, ON, Canada), and A. Carballar (Universidad de Sevilla, Spain).

References

[1] L. Venema, "Photonics technologies," *Nature Insight*, vol. 424, no. 6950, p. 809, Aug. 2003.
[2] J. Azaña, C. K. Madsen, K. Takiguchi, and G. Cincontti, Eds., "Special issue on 'Optical signal processing'," *IEEE/OSA J. Lightwave Technol.*, vol. 24, no. 7, pp. 2484–2767, Jul. 2006.
[3] M. Vasilyev, Y. Su, and C. McKinstrie, Eds., "Special issue on 'Nonlinear optical signal processing'," *IEEE J. Sel. Top. Quantum Electron.*, vol. 14, no. 3, pp. 527–971, May/Jun. 2008.
[4] A. V. Oppenheim, A. S. Willsky, and S. H. Nawab, *Signals and Systems,* 2nd ed. Upper Saddle River, NJ: Prentice-Hall, 1996.
[5] C.-W. Hsue, L.-C. Tsai, and K.-L. Chen, "Implementation of first-order and second-order microwave differentiators," *IEEE Trans. Microw. Theory Tech.*, vol. 52, no. 5, pp. 1443–1448, May 2004.
[6] C.-W. Hsue, L.-C. Tsai, and Y.-H. Tsai, "Time-constant control of microwave integrators using transmission lines," *IEEE Trans. Microw. Theory Tech.*, vol. 54, no. 3, pp. 1043–1047, Mar. 2006.
[7] N. Q. Ngo, S. F. Yu, S. C. Tjin, and C. H. Kam, "A new theoretical basis of higher-derivative optical differentiators," *Opt. Commun.*, vol. 230, no. 1–3, pp. 115–129, Jan. 2004.
[8] M. Kulishov and J. Azaña, "Long-period fiber gratings as ultrafast optical differentiators," *Opt. Lett.*, vol. 30, no. 20, pp. 2700–2702, Oct. 2005.
[9] R. Slavík, Y. Park, M. Kulishov, R. Morandotti, and J. Azaña, "Ultrafast all-optical differentiators," *Opt. Express*, vol. 14, no. 22, pp. 10 699–10 707, Oct. 2006.
[10] F. Zeng and J. Yao, "Ultrawideband impulse radio signal generation using a high-speed electrooptic phase modulator and a fiber-Bragg-grating-based frequency discriminator," *IEEE Photon. Technol. Lett.*, vol. 18, no. 19, pp. 2062–2064, Oct. 2006.
[11] Z. Li, S. Zhang, J. M. Vazquez, Y. Liu, G. D. Khoe, H. J. S. Dorren, and D. Lenstra, "Ultrafast optical differentiators based on asymmetric Mazch-Zehnder interferometer," in *Proc. Symp. IEEE/LEOS*, 2006, pp. 173–176, Benelux Chapter.
[12] N. K. Berger, B. Levit, B. Fischer, M. Kulishov, D. V. Plant, and J. Azaña, "Temporal differentiation of optical pulses using a phase-shifted fiber Bragg grating," *Opt. Express*, vol. 15, pp. 371–381, 2007.
[13] Y. Park, J. Azaña, and R. Slavík, "Ultrafast all-optical first- and higher-order differentiators based on interferometers," *Opt. Lett.*, vol. 32, no. 6, pp. 710–712, Mar. 2007.
[14] M. Kulishov and J. Azaña, "High-order all-optical temporal differentiation using multiple-phase-shifted fiber Bragg gratings," *Opt. Express*, vol. 15, pp. 6152–6166, 2007.

[15] J. Azaña, Y. Park, T.-J. Ahn, and R. Slavík, "All-fiber ultrafast second-order differentiator based on a single uniform long-period fiber grating," presented at the OSA Topical Meeting Bragg Gratings, Photosensitivity, Poling Glass Waveguides, Quebec City, QC, Canada, Sep. 2–7, 2007, Paper JWA42.
[16] L.-M. Rivas, K. Singh, A. Carballar, and J. Azaña, "Arbitrary-order ultra-broadband all-optical differentiators based on fiber Bragg gratings," *IEEE Photon. Technol. Lett.*, vol. 19, no. 16, pp. 1209–1211, Aug. 2007.
[17] M. Kulishov, D. Krcmarík, and R. Slavík, "Design of terahertz-bandwidth arbitrary-order temporal differentiators based on long-period fiber gratings," *Opt. Lett.*, vol. 32, no. 20, pp. 2978–2980, Oct. 2007.
[18] M. A. Preciado, V. García-Muñoz, and M. A. Muriel, "Ultrafast all-optical Nth-order differentiator based on chirped fiber Bragg gratings," *Opt. Express*, vol. 15, no. 12, pp. 7196–7201, 2007.
[19] Y. Dai, X. Chen, H. Ji, and S. Xie, "Optical arbitrary waveform generation based on sampled fiber Bragg gratings," *IEEE Photon. Technol. Lett.*, vol. 19, no. 23, pp. 1916–1918, Dec. 2007.
[20] F. Liu, T. Wang, L. Qiang, T. Ye, Z. Zhang, M. Qiu, and Y. Su, "Compact optical temporal differentiator based on silicon microring resonator," *Opt. Express*, vol. 16, no. 20, pp. 15 880–15 886, Sep. 2008.
[21] M. A. Preciado and M. A. Muriel, "Design of an ultrafast all-optical differentiator based on a fiber Bragg grating in transmission," *Opt. Lett.*, vol. 33, no. 21, pp. 2458–2461, Nov. 2008.
[22] D. Krčmařík, R. Slavík, Y. Park, M. Kulishov, and J. Azaña, "First-order loss-less differentiators using long period gratings made in Er-doped fibers," *Opt. Express*, vol. 17, no. 2, pp. 461–471, Jan. 2009.
[23] C. Cuadrado-Laborde and M. V. Andrés, "In-fiber all-optical fractional differentiator," *Opt. Lett.*, vol. 34, no. 6, pp. 833–835, Mar. 2009.
[24] R. Slavík, Y. Park, D. Krčmaík, and J. Azaña, "Stable all-fiber photonic temporal differentiator using a long-period fiber grating interferometer," *Opt. Commun.*, vol. 282, no. 12, pp. 2339–2342, Jun. 2009.
[25] L.-M. Rivas, S. Boudreau, Y. Park, R. Slavík, S. LaRochelle, A. Carballar, and J. Azaña, "Experimental demonstration of ultrafast all-fiber high-order temporal differentiators," *Opt. Lett.*, vol. 34, no. 12, pp. 1792–1794, Jun. 2009.
[26] M. Li, D. Janner, J. P. Yao, and V. Pruneri, "Arbitrary-order all-fiber temporal differentiator based on a fiber Bragg grating: Design and experimental demonstration," *Opt. Express*, vol. 17, no. 22, pp. 19 798–19 807, Oct. 2009.
[27] R. Slavík, Y. Park, M. Kulishov, and J. Azaña, "THz-bandwidth high-order temporal differentiators based on phase-shifted long-period fiber gratings," *Opt. Lett.*, vol. 34, no. 20, pp. 3116–3118, Oct. 2009.
[28] A. V. Okishev, "Optical differentiation and multimillijoule ~150-ps pulse generation in a regenerative amplifier with a temperature-tuned intracavity volume Bragg grating," *Appl. Opt.*, vol. 49, no. 8, pp. 1331–1334, Mar. 2010.
[29] N. Q. Ngo, "Optical integrator for optical dark-soliton detection and pulse shaping," *Appl. Opt.*, vol. 45, no. 26, pp. 6785–6791, 2006.
[30] N. Q. Ngo and L. N. Binh, "Optical realization of Newton-Cotes-based integrators for dark soliton generation," *J. Lightwave Technol.*, vol. 24, no. 1, pp. 563–572, Jan. 2006.
[31] N. Q. Ngo and L. N. Binh, "New approach for the design of an optical square pulse generator," *Appl. Opt.*, vol. 46, no. 17, pp. 3546–3560, Jun. 2007.
[32] N. Q. Ngo, "Design of an optical temporal integrator based on a phase-shifted fiber Bragg grating in transmission," *Opt. Lett.*, vol. 32, pp. 3020–3022, 2007.
[33] M. H. Asghari and J. Azaña, "Design of all-optical high-order temporal integrators based on multiple-phase-shifted Bragg gratings," *Opt. Express*, vol. 16, no. 15, pp. 11 459–11 469, Jul. 2008.
[34] R. Slavík, Y. Park, N. Ayotte, S. Doucet, T.-J. Ahn, S. LaRochelle, and J. Azaña, "Photonics temporal integrator for all-optical computing," *Opt. Express*, vol. 16, no. 22, pp. 18 202–18 214, Oct. 2008.
[35] Y. Ding, X.-B. Zhang, X.-L. Zhang, and D. Huang, "Proposal for loadable and erasable optical memory unit based on dual active microring optical integrators," *Opt. Commun.*, vol. 281, pp. 5315–5321, Nov. 2008.
[36] J. Azaña, "Proposal of a uniform fiber Bragg grating as an ultrafast all-optical integrator," *Opt. Lett.*, vol. 33, no. 1, pp. 4–6, Jan. 2008.
[37] M. H. Asghari and J. Azaña, "Arbitrary-order temporal integration of ultrafast optical signals using a single uniform-period fiber Bragg grating," *Opt. Lett.*, vol. 33, no. 13, pp. 1548–1550, Jul. 2008.
[38] M. A. Preciado and M. A. Muriel, "Ultrafast all-optical integrator based on a fiber Bragg grating: Proposal and design," *Opt. Lett.*, vol. 33, no. 12, pp. 1348–1350, Jun. 2008.
[39] Y. Park, T.-J. Ahn, Y. Dai, J. Yao, and J. Azaña, "All-optical temporal integration of ultrafast pulse waveforms," *Opt. Express*, vol. 16, no. 22, pp. 17 817–17 825, Oct. 2008.
[40] M. H. Asghari and J. Azaña, "On the design of efficient and accurate arbitrary-order temporal optical integrators using fiber Bragg gratings," *J. Lightwave Technol.*, vol. 27, no. 17, pp. 3888–3895, Sep. 2009.
[41] Y. Ding, X.-B. Zhang, X.-L. Zhang, and D. Huang, "Active microring optical integrator associated with electroabsorption modulators for high speed low light power loadable and erasable optical memory unit," *Opt. Express*, vol. 17, no. 15, pp. 12 835–12 848, Jul. 2009.
[42] Y. Ding, X.-B. Zhang, X.-L. Zhang, and D. Huang, "Raman based silicon photonic integrator," in *Proc. Pacific Rim Conf. Lasers Electro-Optics (CLEO/PACIFIC RIM)*, Shanghai, China.
[43] M. H. Asghari, C. Wang, J. Yao, and J. Azaña, "High-order passive photonic temporal integrators," *Opt. Lett.*, vol. 35, no. 8, pp. 1191–1193, Apr. 2010.
[44] J. Yao, F. Zeng, and Q. Wang, "Photonic generation of ultrawideband signals," *IEEE/OSA J. Lightwave Technol.*, vol. 25, no. 11, pp. 3219–3235, Nov. 2007.
[45] J. Xu, X. Zhang, J. Dong, D. Liu, and D. Huang, "All-optical differentiator based on cross-gain modulation in semiconductor optical amplifier," *Opt. Lett.*, vol. 32, no. 20, pp. 3029–3031, Oct. 2007.
[46] Q. Wang and J. Yao, "Switchable optical UWB monocycle and doublet generation using a reconfigurable photonic microwave delay-line filter," *Opt. Express*, vol. 15, no. 22, pp. 14 667–14 672, Oct. 2007.
[47] J. Xu, X. Zhang, J. Dong, D. Liu, and D. Huang, "High-speed all-optical differentiator based on a semiconductor optical amplifier and an optical filter," *Opt. Lett.*, vol. 32, no. 13, pp. 1872–1874, Jul. 2007.
[48] P. Velanas, A. Bogris, A. Argyris, and D. Syvridis, "High-speed all-optical first- and second-order differentiators based on cross-phase modulation in fibers," *J. Lightwave Technol.*, vol. 26, no. 18, pp. 3269–3276, Sep. 2008.

[49] J. Li, S. Fu, K. Xu, J. Wu, J. Lin, M. Tang, and P. Shum, "Photonic ultrawideband monocyle pulse generation using a single electro-optic modulator," *Opt. Lett.*, vol. 33, no. 3, pp. 288–290, Feb. 2008.
[50] Z. Li and C. Wu, "All-optical differentiator and high-speed pulse generation based on cross-polarization modulation in a semiconductor optical amplifier," *Opt. Lett.*, vol. 34, no. 6, pp. 830–832, Mar. 2009.
[51] M. Bolea, J. Mora, B. Ortega, and J. Capmany, "Optical UWB pulse generator using an N tap microwave photonic filter and phase inversion adaptable to different pulse modulation formats," *Opt. Express*, vol. 17, no. 7, pp. 5023–5032, Mar. 2009.
[52] N. Q. Ngo and L. N. Binh, "Programmable incoherent Newton-Cotes optical integrator," *Opt. Commun.*, vol. 119, no. 3/4, pp. 390–402, Sep. 1995.
[53] Y. Park and J. Azaña, "Ultrafast photonic intensity integrator," *Opt. Lett.*, vol. 34, no. 8, pp. 1156–1158, Apr. 2009.
[54] C. K. Madsen and J. H. Zhao, *Optical Filter Design and Analysis: A Signal Processing Approach*. New York: Wiley, 1999.
[55] A. M. Vengsarkar, P. J. Lemaire, J. B. Judkins, V. Bhatia, T. Erdogan, and J. E. Sipe, "Long-period fiber gratings as band-rejection filters," *J. Lightwave Technol.*, vol. 14, no. 1, pp. 58–65, Jan. 1996.
[56] R. Kashyap, *Fiber Bragg Gratings*, 2nd ed. San Diego, CA: Academic, 2009.
[57] M. J. Strain and M. Sorel, "Integrated III–V Bragg gratings for arbitrary control over chirp and coupling coefficient," *IEEE Photon. Technol. Lett.*, vol. 20, no. 22, pp. 1863–1865, Nov. 2008.
[58] J. Skaar, L. Wang, and T. Erdogan, "On the synthesis of fiber Bragg gratings by layer peeling," *IEEE J. Quantum Electron*, vol. 37, no. 2, pp. 165–173, Feb. 2001.
[59] G. F. Simmons, *Differential Equations With Applications and Historical Notes*, 2nd ed. New York: McGraw-Hill, 1991.
[60] N. Q. Ngo, L. N. Binh, and X. Dai, "Optical dark-soliton generators and detectors," *Opt. Commun.*, vol. 132, no. 3/4, pp. 389–402, Dec. 1996.
[61] Y. Park, M. Kulishov, R. Slavík, and J. Azaña, "Picosecond and sub-picosecond flat-top pulse generation using uniform long-period fiber gratings," *Opt. Express*, vol. 14, no. 26, pp. 12670–12678, Dec. 2006.
[62] M. H. Asghari and J. Azaña, "Proposal and analysis of a reconfigurable pulse shaping technique based on multi-arm optical differentiators," *Opt. Commun.*, vol. 281, no. 18, pp. 4581–4588, Sep. 2008.
[63] F. Li, Y. Park, and J. Azaña, "Complete temporal pulse characterization using phase reconstruction based on optical ultrafast differentiation (PROUD)," *Opt. Lett.*, vol. 32, no. 22, pp. 3364–3366, Nov. 2007.
[64] F. Li, Y. Park, and J. Azaña, "Linear characterization of optical pulses with durations ranging from the picosecond to the nanosecond regime using ultrafast photonic differentiation," *J. Lightwave Technol.*, vol. 27, no. 21, pp. 4623–4633, Nov. 2009.
[65] F. Li, Y. Park, and J. Azaña, "Group delay characterization of dispersive devices using a simple temporal intensity measurement setup," *IEEE Photon. Technol. Lett.*, vol. 20, no. 24, pp. 2042–2044, Dec. 2008.
[66] M. H. Asghari, Y. Park, and J. Azaña, "Demonstration of a photonic integrator-based loadable and erasable optical memory unit with picosecond switching times," in *Proc. 35th Eur. Conf. Optical Commun. (ECOC)*, Vienna, Austria, Sep. 20–24, 2009.
[67] T. Erdogan, "Fiber grating spectra," *J. Lightwave Technol.*, vol. 15, no. 8, pp. 1277–1294, Aug. 1997.
[68] R. Slavík, "Extremely deep long-period fiber grating made with CO_2 laser," *IEEE Photon. Technol. Lett.*, vol. 18, no. 16, pp. 1705–1707, Aug. 2006.
[69] B. H. Kim, T. J. Ahn, D. Y. Kim, B. H. Lee, Y. Chung, U. C. Paek, and W. T. Han, "Effects of CO_2 laser irradiation on the refractive-index change in optical fibers," *Appl. Opt.*, vol. 41, no. 19, pp. 3809–3815, Jul. 2002.
[70] L. Lepetit, G. Chériaux, and M. Joffre, "Linear technique of phase measurement by femtosecond spectral interferometry for applications in spectroscopy," *J. Opt. Soc. Amer. B, Opt. Phys.*, vol. 12, no. 12, pp. 2467–2474, Dec. 1995.
[71] Y. Park, F. Li, and J. Azaña, "Characterization and optimization of optical pulse differentiation using spectral interferometry," *IEEE Photon. Technol. Lett.*, vol. 18, no. 17, pp. 1798–1800, Sep. 2006.
[72] J. Azaña and L. R. Chen, "Synthesis of temporal optical waveforms by fiber Bragg gratings: A new approach based on space-to-frequency-to-time mapping," *J. Opt. Soc. Amer. B, Opt. Phys.*, vol. 19, no. 11, pp. 2758–2769, Nov. 2002.
[73] C. Paré and P. A. Bélanger, "Antisymmetric soliton in a dispersion-managed system," *Opt. Commun.*, vol. 168, no. 1–4, pp. 103–109, Sep. 1999.
[74] M. Stratmann, T. Pagel, and F. Mitschke, "Experimental observation of temporal soliton molecules," *Phys. Rev. Lett.*, vol. 95, no. 14, pp. 143 902-1–143 902-3, Sep. 2005.
[75] P. Petropoulos, M. Ibsen, A. D. Ellis, and D. J. Richardson, "Rectangular pulse generation based on pulse reshaping using a superstructured fiber Bragg grating," *Lightwave Technol.*, vol. 19, no. 5, pp. 746–752, May 2001.
[76] J. H. Lee, P. C. The, P. Petropoulos, M. Ibsen, and D. J. Richardson, "All-optical modulation and demultiplexing systems with significant timing jitter tolerance through incorporation of pulse shaping fiber Bragg gratings," *IEEE Photon. Technol. Lett.*, vol. 14, no. 2, pp. 203–205, Feb. 2002.
[77] F. Parmigiani, P. Petropoulos, M. Ibsen, and D. J. Richardson, "All-optical pulse reshaping and retiming systems incorporating pulse shaping fiber Bragg grating," *J. Lightwave Technol.*, vol. 24, no. 1, pp. 357–364, Jan. 2006.
[78] L. K. Oxenlowe, R. Slavík, M. Galili, H. C. M. Mulvad, A. T. Clausen, Y. Park, J. Azaña, and P. Jeppesen, "640 Gb/s timing jitter tolerant data processing using a long-period fiber grating-based flat-top pulse shaper," *IEEE J. Sel. Topics Quantum Electron.*, vol. 14, no. 3, pp. 566–572, May/Jun. 2008.
[79] L. R. Chen, S. D. Benjamin, P. W. E. Smith, and J. E. Sipe, "Ultrashort pulse reflection from fiber gratings: A numerical investigation," *J. Lightwave Technol.*, vol. 15, no. 8, pp. 1503–1512, Aug. 1997.
[80] Y. Park, M. H. Asghari, T.-J. Ahn, and J. Azaña, "Transform-limited picosecond pulse shaping based on coherence synthesization," *Opt. Express*, vol. 15, no. 15, pp. 9584–9599, Jul. 2007.